



This discussion paper is/has been under review for the journal Atmospheric Chemistry and Physics (ACP). Please refer to the corresponding final paper in ACP if available.

New emission factors for Australian vegetation fires measured using open-path Fourier transform infrared spectroscopy – Part 1: methods and Australian temperate forest fires

C. Paton-Walsh¹, T. E. L. Smith², E. L. Young¹, D. W. T. Griffith¹, and É.-A. Guérette¹

¹Centre for Atmospheric Chemistry, School of Chemistry, University of Wollongong, Wollongong, New South Wales, Australia

²Department of Geography, King's College London, Earth and Environmental Dynamics Research Group, Strand, London, WC2R 2LS, UK

Received: 11 November 2013 – Accepted: 30 January 2014 – Published: 18 February 2014

Correspondence to: C. Paton-Walsh (clarem@uow.edu.au)

Published by Copernicus Publications on behalf of the European Geosciences Union.

New emission factors for Australian vegetation fires

C. Paton-Walsh et al.

Title Page

Abstract

Introduction

Conclusions

References

Tables

Figures



Back

Close

Full Screen / Esc

Printer-friendly Version

Interactive Discussion



Abstract

Biomass burning releases trace gases and aerosol particles that significantly affect the composition and chemistry of the atmosphere. Australia contributes approximately 8 % of gross global carbon emissions from biomass burning, yet there are few previous measurements of emissions from Australian forest fires available in the literature. This paper describes the results of field measurements of trace gases emitted during hazard reduction burns in Australian temperate forests using open-path Fourier transform infrared spectroscopy. In a companion paper, similar techniques are used to characterise the emissions from hazard reduction burns in the savanna regions of the Northern Territory. Details of the experimental methods are explained, including both the measurement set-up and the analysis techniques employed. The advantages and disadvantages of different ways to estimate whole-fire emission factors are discussed and a measurement uncertainty budget is developed.

Emission factors for Australian temperate forest fires are given for the first time for many trace gases. We recommend the following emission factors for Australian temperate forest fires (in grams of gas emitted per kilogram of dry fuel burned) which are our mean measured values: 1620 g kg⁻¹ of carbon dioxide; 118 g kg⁻¹ of carbon monoxide; 3.5 g kg⁻¹ of methane; 1.3 g kg⁻¹ of ethylene; 1.7 g kg⁻¹ of formaldehyde; 2.4 g kg⁻¹ of methanol; 3.8 g kg⁻¹ of acetic acid; 0.4 g kg⁻¹ of formic acid; 1.7 g kg⁻¹ of ammonia; 0.15 g kg⁻¹ of nitrous oxide and 0.5 g kg⁻¹ of ethane.

1 Introduction

Vegetation fires are a huge source of trace gases to the atmosphere, second only to fossil fuel combustion in their contribution to total global carbon emissions, with major implications for atmospheric chemistry on a global scale. On local to regional scales, the emissions from biomass burning can degrade air quality and impact negatively on human health. In Australia, average annual gross emissions of carbon from fires

ACPD

14, 4327–4381, 2014

New emission factors for Australian vegetation fires

C. Paton-Walsh et al.

Title Page

Abstract

Introduction

Conclusions

References

Tables

Figures

◀

▶

◀

▶

Back

Close

Full Screen / Esc

Printer-friendly Version

Interactive Discussion



New emission factors for Australian vegetation fires

C. Paton-Walsh et al.

[Title Page](#)[Abstract](#)[Introduction](#)[Conclusions](#)[References](#)[Tables](#)[Figures](#)[Back](#)[Close](#)[Full Screen / Esc](#)[Printer-friendly Version](#)[Interactive Discussion](#)

measured from different ecosystems. They included as many measurements as were available at the time, converting measurements of ratios of different gases to equivalent emission factors for these gases where necessary. More recently, Akagi et al. (2011) produced an updated version that only included measurements made directly at the fires, excluding so called “enhancement ratios” measured down-wind of the fires. Both compilations report a very wide range of emission factors for individual ecosystems. This reflects both natural variability (driven by differences in vegetation cover, moisture content and fire intensity) and potential sampling biases from different studies that derive from different measurement geometries (as explained below).

Vegetation fires can be thought of as burning in two main stages: flaming and smouldering. Flaming combustion results in larger proportions of highly oxidised species such as CO₂, whilst emissions from smouldering combustion contain more CO and volatile organics. For this reason, the emission factors depend on the balance of flaming and smouldering combustion that occurs throughout the fire (Andreae and Merlet, 2001). Species emitted during the rapid and intense flaming stage are lofted by convection, whilst many other trace gases are emitted predominantly through the slow and sometimes prolonged smouldering stage.

Ideally, sampling techniques should capture a representative amount of flaming and smouldering combustion so that the measurements are representative of the fire as a whole. Care must also be taken in the choice of method of combining measurements to get the best estimate for fire-averaged emission factors (see Sect. 2.2). Ground-based in situ measurements may be biased towards the smouldering stage of burning since flaming emissions are transported rapidly to higher altitudes via convection. Aircraft-based measurements capture both flaming and smouldering emissions lofted during the initial stages of the fire but have very limited temporal coverage and therefore may underestimate the smouldering emissions. Laboratory burns are also potentially biased toward flaming combustion as the limited mass burned in experiments means that the smouldering stage may be curtailed.

**New emission factors
for Australian
vegetation fires**

C. Paton-Walsh et al.

Title Page

Abstract

Introduction

Conclusions

References

Tables

Figures

◀

▶

◀

▶

Back

Close

Full Screen / Esc

Printer-friendly Version

Interactive Discussion



are a number of other studies that present enhancement ratios measured in aged smoke using either ground-based solar remote sensing Fourier transform spectrometry or satellite-based spectroscopic measurements (Glatthor et al., 2013; Paton-Walsh et al., 2005, 2004; Young and Paton-Walsh, 2011). For conversion to an equivalent emission factor, these measured enhancement ratios require an assumed emission factor for CO which introduces large uncertainties to the emission factors for these fires. Additionally, concentrations of gases have been measured in smoke from Australian forest fires to assess the exposure levels of fire-fighters and rural populations exposed to bushfire smoke (Reisen and Brown, 2009; Reisen et al., 2011). A study that identified emissions from eucalyptus species at high temperatures and during combustion produced no quantitative mole fractions, nor any emission factors (Maleknia et al., 2009).

The work described in this paper aims to contribute to the sparse base of knowledge concerning the atmospheric emissions from Australian temperate forest fires. Open-path FTIR spectroscopy was used for field measurements of trace gases emitted during five different hazard reduction burns in Australian temperate forests in 2010 and 2012. In a partner paper, similar techniques are employed to provide new emission factors from Australian savanna fires (Smith et al., 2013).

2 Methods for calculating emission factors

2.1 Calculating emission factors and modified combustion efficiency

The emission factor (EF_i) is the mass of a gaseous species (i) emitted per unit of dry fuel consumed, usually expressed in units of g kg^{-1} . When the measurements include the species that contain the majority of the carbon that is emitted by the fires, then approximate emission factors for each of the trace gases of interest can be calculated

using the method previously used by Ward and Radke (1993):

$$EF_i = F_c \times 1000 \times \frac{MM_i}{12} \times \frac{C_i}{C_T} \quad (1)$$

where EF_i is the mass in grams of species i emitted per kilogram of dry fuel burned, (g kg^{-1}); F_c is the fractional carbon content of the fuel (assumed here to be 0.50 ± 0.05 for all hazard reduction burns, Yokelson et al., 1999a); MM_i is the molecular mass of species i and 12 is the atomic mass of carbon; C_i/C_T is the number of moles of species i emitted divided by the total number of moles of carbon emitted, and may be calculated directly from excess mole fractions measured according to Eq. (2):

$$\frac{C_i}{C_T} = \frac{\Delta[i]}{\sum_{j=1}^n (NC_j \times \Delta[j])} \quad (2)$$

where $\Delta[i]$ and $\Delta[j]$ are the excess mole fractions of species i and j respectively (defined as the mole fraction e.g. $[i]$ measured in the smoke, minus the mean background mole fraction measured before the fire $[i]_{\text{bkgrnd}}$), NC_j is the number of carbon atoms in compound j and the sum is of all carbon containing species emitted by the fire. Only those carbonaceous species retrieved in this work (CO_2 , CO , CH_4 , C_2H_4 , H_2CO , CH_3OH , HCOOH and CH_3COOH) have been included in the emission factor calculations. Whilst these do not represent all of the carbon-containing species emitted by a fire, they do account for the vast majority of carbon emissions ($\sim > 98\%$). Most of the carbon emitted by biomass burning is in the form of CO_2 and CO (90–95%), the remaining as CH_4 or other volatile organic carbon compounds and particulate matter (Akagi et al., 2011). Use of only those carbonaceous species detected by FTIR spectrometry in this mass balance equation has been estimated to artificially inflate the emission factors by 1–2% (Yokelson et al., 2007).

C_i/C_T may also be calculated using emission ratios with respect to a reference species (usually CO_2 or CO) via Eqs. (3) and (4):

$$\frac{C_i}{C_T} = \frac{\text{ER}(i/\text{CO}_2)}{\sum_{j=1}^n (\text{NC}_j \times \text{ER}(j/\text{CO}_2))} \quad (3)$$

where $\text{ER}_{i/y}$ is the emission ratio of species i to the reference species y , given by:

$$\text{ER}_{i/y} = \frac{\Delta[i]}{\Delta[y]} = \frac{[i] - [i]_{\text{bkgnd}}}{[y] - [y]_{\text{bkgnd}}} \quad (4)$$

where $\Delta[i]$ is the excess mole fraction of species i . (Note that when the measurements are made downwind of the fire in aged smoke, then these same ratios are commonly referred to as “enhancement ratios”, to highlight the fact that chemical and physical processing may have altered the ratio of species from that which was originally emitted from the fire). Deriving the emission ratios via the gradient of the linear best fit to a plot of the abundance of species i against the abundance of reference species y , removes the requirement for accurate knowledge of the background mole fractions, yet introduces an insignificant degree of error (Wooster et al., 2011).

The emission factor for a particular species may then be calculated via Eq. (5):

$$\text{EF}_i = \text{ER}_{i/y} \times \frac{\text{MW}_i}{\text{MW}_y} \times \text{EF}_y \quad (5)$$

where EF_i is the emission factor of species i (gkg^{-1}), MM_i and MM_y are the molecular weights of species i and species y respectively, EF_y is the emission factor of the reference species y .

Since an excess mole fraction for each of the gases is retrieved from every spectrum recorded during the fire, it is possible to calculate a separate emission factor for each

gas from every spectrum. However, emission factors of some gases may change as the fire develops depending upon the combustion efficiency of the material being burned. The combustion efficiency is defined as the proportion of total carbon emitted as CO₂ and is now commonly approximated to a modified combustion efficiency (MCE) given by Eq. (6) (Hao and Ward, 1993; Yokelson et al., 1996):

$$\text{MCE} = \frac{\Delta[\text{CO}_2]}{\Delta[\text{CO}_2] + \Delta[\text{CO}]} \quad (6)$$

When the fire is dominated by flaming combustion, the combustion efficiency is high. It decreases as smouldering combustion becomes more dominant.

2.2 Obtaining best-estimates for fire-averaged emission factors

One consequence of the fact that many emission factors change with combustion efficiency as the fire develops is that a measurement made at one stage of the fire may not be representative of the fire as a whole. There are a number of different ways in which whole-fire emissions estimates can be made, each with its own advantages and disadvantages, and these are outlined below:

1. Arithmetic mean: the simplest method is to calculate separate emission factors for each spectrum independently and to take a simple arithmetic mean. The problem with this approach is that it fails to account for the larger rate of biomass consumption during flaming combustion (Akagi et al., 2011). Thus weighting all the spectra equally will result in an unwanted dependence on the relative time spent measuring during flaming and smouldering combustion. Since flaming combustion is relatively quick this will bias the estimated fire-averaged emission factors towards smouldering emissions compared to the true overall emissions.
2. Regression to CO₂: a different method is to calculate emission ratios to CO₂ for each species from the relevant regressions. Emission factors may then be calculated using Eqs. (1) and (3) that use the data from all spectra together. This

New emission factors for Australian vegetation fires

C. Paton-Walsh et al.

Title Page

Abstract

Introduction

Conclusions

References

Tables

Figures



Back

Close

Full Screen / Esc

Printer-friendly Version

Interactive Discussion



New emission factors for Australian vegetation fires

C. Paton-Walsh et al.

Title Page

Abstract

Introduction

Conclusions

References

Tables

Figures



Back

Close

Full Screen / Esc

Printer-friendly Version

Interactive Discussion



- to 68 % of fuel consumed in flaming and 32 % in smouldering combustion. In the absence of fire radiative power measurements, the issue of what proportion of flaming and smouldering combustion occurred in the fire as a whole may be left unanswered. Without an estimate of the relative amounts of fuel consumed within these MCE ranges, an estimate of the whole-fire emission factor cannot be made.
- 5
4. Summation Method: a good way to ensure that the fire-averaged emission factor correctly weights each spectrum to the total biomass consumed is to calculate the total excess amounts of each gas detected by summing the excess amounts from each spectrum. The emission factors may then be calculated for the whole fire via Eqs. (1) and (2). This method has the significant advantage that it correctly weights each spectrum by the proportion of the total sampled excess carbonaceous species measured, with the only drawback being that it relies on accurate knowledge of background mole fractions. This method has been used for laboratory fires where the geometry of the measurement set-up ensures that the whole fire has been sampled in a representative manner (since spectra are recorded throughout all stages of the burn, from flaming until the smouldering combustion is finally extinguished and with the flow rate controlled through the sample path, Burling et al., 2010). In our measurements, we cannot be sure that we have sampled a representative amount of flaming and smouldering combustion in the fire. This will depend upon the geometry of our measurement set-up (line of sight) and local meteorological conditions (e.g. a significant change in wind-strength or direction between flaming and smouldering might also produce sampling biases). Nevertheless, in many instances our measurement geometry is such that we have an excellent chance of capturing a representative sample of flaming and smouldering emissions and any sampling bias should be small. In such cases, our measured sample is our best estimate of the true emissions from the fire.
- 10
- 15
- 20
- 25
5. Emission Ratio to Reference Gas: emission factors may also be calculated via Eq. (5) using the measured emission ratio of the gas of interest with respect to

New emission factors for Australian vegetation fires

C. Paton-Walsh et al.

Title Page

Abstract

Introduction

Conclusions

References

Tables

Figures



Back

Close

Full Screen / Esc

Printer-friendly Version

Interactive Discussion



a reference species (usually CO or CO₂). Using the gradient of a regression line between the target gas and the reference gas will often yield the emission ratio with very low uncertainty, which is a significant advantage of this method. This method is sometimes used with an assumed value for the emission factor of the reference species (usually taken from a previous study or mean literature value for the ecosystem) which can introduce large extra uncertainties. However in this case the emission factors of CO₂ and CO can be derived directly from the measurements and so no such disadvantage is present.

In this study, we have chosen to use a combination of methods 4 and 5 above to calculate whole fire emission factors. We have used the whole fire summation method to obtain our best estimate for the emission factors of CO₂ and CO, using the background mole fraction values for these gases measured before ignition of the fires. For all other gases (where the background values are often closer to the quantitation limits of the measurement technique), we have used emission ratios via Eq. (5) and the emission factors for CO₂ and CO calculated for the fire via the summation method. The reference species used for each of the emission factor calculations was chosen based upon which species (CO or CO₂) was more strongly correlated to the particular trace gas *i*; C₂H₄, H₂CO and N₂O were most strongly correlated to CO₂ whereas all other gases were most strongly correlated to CO.

3 Open-path Fourier transform infrared spectroscopic measurement techniques

3.1 The open-path FTIR system

The open-path FTIR system operated by the University of Wollongong consists of a Bomem MB-100 Series FTIR spectrometer (1 cm⁻¹ resolution), fitted with a Meade 12'' (305 mm) LX200 telescope. The spectrometer is equipped with a built-in infrared

source so that the infrared radiation is modulated within the spectrometer before being sent out through the telescope to the distant retro-reflectors, typically located 20 to 50 m away. It is then returned through the telescope – and the fraction of the radiation that is reflected by the external beam splitter is focused onto the detector (see Fig. 1) (Phillips et al., 2011).

This “monostatic” configuration, shown in Fig. 1, has significant advantages over the more commonly used “bistatic” configuration (where a distant collimated infrared source is imaged by a telescope onto the entrance aperture of the spectrometer) (Akagi et al., 2013; Goode et al., 1999; Griffith et al., 1991; Smith et al., 2011; Wooster et al., 2011) because there is no requirement to correct for radiation emitted by the surrounding environment, (see Bacsik et al., 2004). This is because the radiation from the surrounding environment is not modulated in this arrangement and therefore appears only as a direct current signal on the detector (and thus has no significant impact on the resulting spectrum). Pre-modulation of the radiation source is especially important when wanting to measure flaming combustion because the strong radiation source emitted by the flames is not seen at the detector. Our monostatic configuration allows measurement even through flames thereby avoiding any potential bias that might result from targeting predominantly smouldering emissions.

The detector used in this study was a liquid nitrogen cooled Mercury Cadmium Telluride (MCT) detector. The spectrometer was mounted on a tripod such that the line of sight was approximately 1.5 m above the ground and aligned with a retro reflector positioned in the field (typically between 20 m and 40 m from the spectrometer). Single beam spectra were recorded approximately every 20 s (by co-adding 3 scans per spectrum) before and during each burn at 1.0 cm^{-1} resolution.

3.2 Quantitative analysis of infrared spectra

Trace gas mole fractions were calculated from all open-path FTIR spectra using the Multiple Atmospheric Layer Transmission (MALT) program (Griffith, 1996). MALT calculates “synthetic” spectra to closely match measured spectra using an initial estimate

New emission factors for Australian vegetation fires

C. Paton-Walsh et al.

Title Page

Abstract

Introduction

Conclusions

References

Tables

Figures



Back

Close

Full Screen / Esc

Printer-friendly Version

Interactive Discussion



**New emission factors
for Australian
vegetation fires**C. Paton-Walsh et al.

[Title Page](#)[Abstract](#)[Introduction](#)[Conclusions](#)[References](#)[Tables](#)[Figures](#)[⏪](#)[⏩](#)[◀](#)[▶](#)[Back](#)[Close](#)[Full Screen / Esc](#)[Printer-friendly Version](#)[Interactive Discussion](#)

of the amount of each gas present in the measurement path, as well as a combination of absorption line parameters (from the 2008 HITRAN database for this work) (Rothman et al., 2009). The synthetic spectra are iteratively recalculated (using a non-linear least squares method that adjusts the estimated amount of each species present) until the difference between the measured spectra and the synthetic spectra is minimized (the best fit is achieved). A more comprehensive description of the workings of MALT can be found in Griffith (1996) and Griffith et al. (2012).

The MALT model also requires environmental parameters (temperature and pressure) along with parameters that describe the spectrometer and the resulting instrument line-shape in order to calculate the synthetic spectrum. Each of these instrument parameters may be fixed or fitted during the retrieval process. If an instrument parameter is fitted, then the initially assigned value is also adjusted (along with the trace gas mole fractions) such that the final value minimises the difference between the measured and simulated spectra.

In this study, the Bomem MB-100 Series FTIR spectrometer was modelled using a resolution of 0.96 cm^{-1} (fixed), a field of view of 22 milli-radians (fixed), with a Hamming apodisation function applied to match the apodisation applied to the measured spectra. The spectrometer had a few imperfections that resulted in a non-ideal instrument line-shape. An imperfect alignment causes a phase error and shifts the wavenumber scale from the true line positions that are listed in the HITRAN database. The phase error was assigned an initial value of -2° and the wavenumber shift assigned an initial value of 0.1 cm^{-1} and both these parameters were fitted during the retrieval. An empirical asymmetry function was applied to the MALT simulated spectra in order to replicate the actual instrument line-shape better (in addition to fitting a phase error).

Imperfect alignment also causes a broadening of the line-widths of absorbing gases. This additional broadening is described by an instrument parameter called the “effective apodisation”. This is a trapezoidal apodisation function varying from zero (equivalent to a boxcar function for a perfectly aligned instrument) to a value of one (representing a triangular apodisation function). This parameter was fitted for the retrieval of some

**New emission factors
for Australian
vegetation fires**C. Paton-Walsh et al.

[Title Page](#)[Abstract](#)[Introduction](#)[Conclusions](#)[References](#)[Tables](#)[Figures](#)[⏪](#)[⏩](#)[◀](#)[▶](#)[Back](#)[Close](#)[Full Screen / Esc](#)[Printer-friendly Version](#)[Interactive Discussion](#)

trace gases (to obtain the best possible fit) and fixed for others, particularly weak absorbers (in order to ensure a stable fit). Finally, in fitting the simulated spectrum to the measured spectrum, MALT can allow different degrees of freedom in fitting the continuum level (i.e. the intensity of radiation at each wavenumber with no absorption lines present). In most of the spectral regions used in this study, a 2nd order polynomial fit to the continuum level was used (allowing for some non-linear variation of the optical transmission across the wavenumber range used).

The use of synthetic spectra has been proven as an accurate method for quantitative trace gas analysis over a broad range of mole fractions, ranging from those found in the ambient atmosphere to those in highly polluted atmospheres such as biomass burning smoke plumes (Smith et al., 2011). In that study Smith et al. (2011) compared MALT trace gas retrieved amounts from spectra collected using open-path FTIR spectroscopy to true known amounts, reporting MALT retrievals accurate to within 5 % of the true amounts when the environmental parameters are accurately specified. MALT also uses the values of pressure, temperature and path-length provided to convert from the retrieved path-length amounts to mole fraction of each species, usually expressed in $\mu\text{mol mol}^{-1}$ (ppm) or nmol mol^{-1} (ppb).

3.3 Standardised spectral regions and parameters for quantitative analysis of trace gases in highly polluted environments

As part of this study, we have defined a set of standardised spectral regions that can be used for each of the trace gases of interest. This was done with spectra from the monostatic configuration described above and spectra from the bistatic instrument configuration used in the savanna fires and described in our partner paper (Smith et al., 2013). We have chosen spectral windows and fitting parameters that optimise the stability of the retrieval and minimise the residuals to the fits (the differences between the measured and the best fitted synthetic spectra) for these two very different instrumental set-ups. We expect that the standardised spectral regions and fitting parameters

presented would be suitable for use by any other groups employing open-path FTIR spectrometry to measure in similar highly polluted atmospheric environments.

The spectral regions are chosen to contain the most sensitive absorption features of the trace gases of interest (i.e. neither too weak to be detected above the spectral noise of the continuum level, nor too saturated to change with the further addition of more absorbing molecules). The chosen regions are similar but not identical to those used in Akagi et al. (2013). Any unavoidable interfering species that were absorbing in the specified spectral region were accounted for by fitting them at the same time. The standardised spectral regions chosen for each trace gas of interest in this work are described below and summarised in Table 1, with typical fits achieved shown in Fig. 2.

3.3.1 Standardised spectral region for fitting carbon dioxide and carbon monoxide

Carbon dioxide exhibits strong infrared absorptions, even at ambient mole fractions. Unfortunately, the vibrational-rotational band for the asymmetric stretch of the main isotope of carbon dioxide ($^{12}\text{CO}_2$) is saturated at current background amounts (~ 394 ppm). This makes carbon dioxide surprisingly difficult to retrieve accurately from the type of infrared spectra recorded here. Many spectral regions were trialled during this study and these tests showed that a poorly chosen spectral region can introduce inaccuracies of up to 20%. In the end, the region from $2080\text{--}2270\text{ cm}^{-1}$ was chosen for the retrieval of CO_2 and CO from the spectra recorded through smoke at the hazard reduction burns. Nitrous oxide (N_2O) and water (H_2O) are also fitted as interfering absorbers in this window. The phase error and effective apodisation are adjusted during the non-linear least squares fitting retrieval and a 2nd order polynomial fit to the continuum level is allowed. This spectral region (from $2080\text{--}2270\text{ cm}^{-1}$) is reliant on the sensitivity provided by absorption bands of the second most abundant isotope ($^{13}\text{CO}_2$). Photosynthesis results in proportionally less ^{13}C in the vegetation that is burning than in the atmosphere, so reliance on $^{13}\text{CO}_2$ is likely to introduce a negative bias of between 0.5% and 2% depending on the type of vegetation and its main photosyn-

Title Page

Abstract

Introduction

Conclusions

References

Tables

Figures

◀

▶

◀

▶

Back

Close

Full Screen / Esc

Printer-friendly Version

Interactive Discussion



**New emission factors
for Australian
vegetation fires**

C. Paton-Walsh et al.

Title Page

Abstract

Introduction

Conclusions

References

Tables

Figures

◀

▶

◀

▶

Back

Close

Full Screen / Esc

Printer-friendly Version

Interactive Discussion



thetic pathway. These biases are small compared to the total uncertainties (discussed in detail later) and no attempt is made to correct for them. Comparisons show that mole fractions derived from this region are in good agreement (always < 5 %) with the results given by the region from 3520–3775 cm⁻¹, which includes strong features for both ¹²CO₂ and ¹³CO₂. This latter region also has very strong H₂O absorption and this leads to low signal to noise and lower precision. For this reason, the 3520–3775 cm⁻¹ window was used only to confirm the accuracy of the chosen region for highly polluted atmospheres.

The accuracy of this retrieval method was tested using a series of dilutions of a calibration mixture (containing 1 % of each of CO₂, CO, CH₄, C₂H₂, C₂H₄ and C₂H₆) measured with a White cell with an optical path of 22.2 m, coupled to a Bomem MB-100 Series FTIR spectrometer similar to that used for the open-path measurements. The results showed that the spectral region from 3520–3775 cm⁻¹ (with the strong CO₂ and H₂O absorptions) produced CO₂ mole fractions within 1 % of the true known calibration values. For very low mole fractions of CO₂ (ambient levels and below in the 22.2 m White cell) the chosen region (from 2080–2270 cm⁻¹) failed to retrieve accurate mole fractions. This was due to the combination of a short path-length, low pressure and unusually low mole fractions producing very weak absorption features. However, within the range of absorbances used before and during the fires, the results are consistent between the two regions demonstrating accuracy within 5 %. CO mole fractions retrieved from chosen spectral region (from 2080–2270 cm⁻¹) were within 2 % of the true known calibration values. It should be noted that these uncertainties are only one contributor to the total uncertainty budget, which is described in detail later in this paper. These results for the calibration of CO₂ and CO are consistent with the open-path calibration results of Smith et al. (2011).

More details of the calibration procedure is given in (Guérette and Paton-Walsh, 2014) which also reports emission factors for volatile organic species from some of these fires, from grab samples measured on a selective ion flow tube mass spectrometer.

3.3.2 Standardised spectral regions and parameters for fitting other trace gases

A single standardised region was chosen to fit ethylene (C_2H_4) and ammonia (NH_3) together from $920\text{--}1000\text{ cm}^{-1}$, with water also retrieved as an interfering species. Phase error and effective apodisation were both adjusted during the retrieval to optimise the fit, and the continuum level was fitted using a 2nd order polynomial.

Standardised regions fitting phase error, effective apodisation and a 2nd order polynomial to the continuum level were also chosen for methane (CH_4) from $2980\text{--}3105\text{ cm}^{-1}$, (with H_2O also retrieved) and for formic acid ($HCOOH$) from $1060\text{--}1150\text{ cm}^{-1}$ with H_2O and NH_3 also retrieved as interfering species. It should be noted that this relatively wide window from $1060\text{--}1150\text{ cm}^{-1}$ incorporates P, Q and R branches of $HCOOH$ and gave significantly better fits to the spectra showing the highest mole fractions (i.e. the smokiest spectra), fitting the NH_3 interference and the continuum level curvature much better than a narrower window ($1098\text{--}1114\text{ cm}^{-1}$) trialled first.

Both methanol (CH_3OH) and formaldehyde (H_2CO) were retrieved fitting only the phase error (with the effective apodisation fixed at zero since this produced a more stable fit for these broad absorbers), and a 2nd order polynomial fitted to the continuum level. The spectral region fitted to retrieve H_2CO was $2710\text{--}2810\text{ cm}^{-1}$ with interfering H_2O also retrieved and from $920\text{--}980\text{ cm}^{-1}$ for CH_3OH with H_2O and NH_3 also fitted as interfering species.

Acetic acid (CH_3COOH) is not available in the HITRAN database and so a library spectrum was used as the basis function for the absorption coefficients (Hurst et al., 1996; Sharpe et al., 2004). Both phase error and effective apodisation were fitted but only a simple slope in continuum level was permitted in the fit because a 2nd order polynomial fit to the continuum level interfered with the correct retrieval of the shallow absorption of acetic acid. The region chosen was $1130\text{--}1230\text{ cm}^{-1}$ and H_2O , NH_3 and $HCOOH$ were fitted as interfering species.

**New emission factors
for Australian
vegetation fires**

C. Paton-Walsh et al.

Title Page

Abstract

Introduction

Conclusions

References

Tables

Figures

◀

▶

◀

▶

Back

Close

Full Screen / Esc

Printer-friendly Version

Interactive Discussion



The region from 2971–3002 cm^{-1} was used to fit weak C_2H_6 absorption features, fitting H_2O , CH_4 and C_2H_4 as interfering species, a 2nd order polynomial fitted to the background and allowing only the phase to vary (with the effective apodisation fixed since this produced a more stable retrieval for this weak absorber). The absorption features were too weak in most spectra to produce a stable fit and so results are provided from a single fire where the strongest trace gas enhancements were measured.

Table 1 summarises all the spectral regions and parameters used in this study, along with another region from 710–760 cm^{-1} used to derive acetylene (C_2H_2) and hydrogen cyanide (HCN) in spectra recorded at savanna burns in Northern Australia and reported in the partner paper (Smith et al., 2013). These gases could not be retrieved from the spectra measured in this study because the particular MCT detector used had insufficient sensitivity in this spectral region. (MCT detectors have different optical cut-offs and the sensitivity of the MCT used in the savanna fires study extends to longer wavelengths than the one used for the forest fires described in this paper).

Example fits for all of the spectral regions used are given in Fig. 2.

4 Hazard reduction burns

In total five hazard reduction burns were attended in this study, with two fires in 2010 and three in 2012. All fires were located in New South Wales (NSW) and were conducted by the NSW National Parks and Wildlife Service often with the assistance of volunteer rural fire services. 2011 was a year with unusually high rainfall (Cottrill, 2012; Tobin and Skinner, 2012) and despite several burns planned in the region no fires were successfully sampled. Vegetation types burned in this study included eucalypt woodland forest, banksia/hakea heath and sclerophyll forest, shrub and woodland. Estimated fuel loadings (before the fires) varied from 8–10 tonnes per hectare (t ha^{-1}) to 20–25 t ha^{-1} and the total area burned varied from 4.8 ha to as much as 148.5 ha (S. Evans, personal communication, 2012, New South Wales Parks and Recreation Service). In all instances only a subset of the total fuel burned could be sampled by the

methods described here with measurements made over several hours and in one case spanning two days of burning.

A brief overview of each fire attended is given below and the main details are summarised in Table 2.

5 4.1 Lane Cove hazard reduction burn

The first hazard reduction burn measurements were made on the 31 August 2010 at Max Allen Drive – the smallest of the burns attended. 4.8 ha of dry sclerophyll open woodland was burned extending outwards from the NSW Parks and Wildlife Service's depot at Lane Cove (33.79° S, 151.15° E). Estimated fuel loading prior to the burn was between 18 and 26 t ha⁻¹. The spectrometer was positioned at the bottom of a steep slope at the depot itself, with the telescope pointing up the hill towards the retro reflector array positioned ~ 53 m away at the edge of the access road. (The total optical path-length from infrared source to detector was estimated to be 107 ± 2 m). The geometric arrangement was such that both smoke and flames passed through the line of sight, making the pre-modulated source essential for this set-up (see Fig. 3a).

4.2 Turramurra hazard reduction burn

The second of the burns attended was at Gibberagong, North Turramurra in Ku-Ring-Gai Chase National Park on the 28 September 2010. This was the largest of all the hazard reduction burns attended in this study, with a total of 148.5 ha of banksia and hakea heath and sclerophyll shrub forest burned (with an estimated fuel loading of 20–25 tonnes per hectare). Over 50 fire-fighters, 3 fire-engines and two helicopters were deployed for the fire with one helicopter dropping incendiary bombs and the other water bombing to prevent the spread of the fire beyond the intended boundaries of the burn.

The spectrometer's telescope and retro-reflectors were set up ~ 42 m apart on a fire trail at the perimeter of the fire-ground and downwind of the flames (see Fig. 3b), with

ACPD

14, 4327–4381, 2014

New emission factors for Australian vegetation fires

C. Paton-Walsh et al.

Title Page

Abstract

Introduction

Conclusions

References

Tables

Figures

◀

▶

◀

▶

Back

Close

Full Screen / Esc

Printer-friendly Version

Interactive Discussion



a total path-length of 84 ± 2 m. This geometry required the smoke to be blown into the measurement path nearby and as such may be biased towards smouldering combustion since some of the emissions from flaming stages of the burn may have been lofted by convection above the line of sight of the spectrometer. However, for a significant part of the measurement period, there was flaming combustion of vegetation on the edge of the fire trail where the spectrometer and retro-reflector were positioned such that some flaming combustion emissions were sampled.

4.3 Aberoo Creek hazard reduction burn

The Aberoo Creek hazard reduction burn took place over two consecutive days (11–12 May 2012) in Heathcote National Park. Approximately 115 ha of shrubby dry sclerophyll forest/heathland was burned over the two days with an estimated fuel loading prior to burning of 12.5 tonnes per hectare.

The northern end of the fire-ground (34.10° S, 150.99° E) was ignited on the 11 May, and the spectrometer and retro-reflectors were set-up 43 m apart (86 m path-length) on the side of the main road into Sydney from the south that bounded the fire-ground downwind of and adjacent to the fires (see Fig. 3c). Further ignition was achieved by the use of incendiary devices dropped from a helicopter flying overhead. Smoke and flames from nearby tea-trees crossed the measurement path fanned by winds from the north west. The proximity to the road could also have produced some interfering pollution from cars slowed by traffic controllers and the smoke blowing across the road.

The southern end of the Aberoo Creek fire-ground (34.13° S, 150.99° E) was ignited on the 12 May. The spectrometer and retro-reflectors were set-up 31 m apart (62 m path-length) at the muster point on the fire trail close to the ignition point. The muster point was an open area of approximately 100 m length and 30 m width with the fires being burned either side.

Vegetation to the east of our measurement path was ignited first and at the time of ignition there was a slight westerly breeze so that little of the emissions from this area were sampled by the spectrometer. Unfortunately, the breeze had dropped away by

New emission factors for Australian vegetation fires

C. Paton-Walsh et al.

Title Page

Abstract

Introduction

Conclusions

References

Tables

Figures

◀

▶

◀

▶

Back

Close

Full Screen / Esc

Printer-friendly Version

Interactive Discussion



the time the area to our west was ignited so our line of path was not ideally located downwind of the burning vegetation (see Fig. 3d). Nevertheless significant enhanced mole fractions were measured along the optical path allowing emission factors to be calculated, but we suspect a bias towards smouldering combustion. Results from both days of burning at Aberoo Creek have been combined in an attempt to yield a more representative sample of flaming and smouldering combustion.

4.4 Gulguer Nature Reserve, hazard reduction burn

Gulguer Nature Reserve, (33.95° S, 150.62° E) is an area of open eucalypt woodland forest with a grassy understorey. The hazard reduction burn took place on 16 May 2012 with the spectrometer and telescope located on a fire trail and the retro-reflectors placed 19 m away (38 m path-length) within the woodland area being burned (see Fig. 3e). In this geometry flaming and smouldering emissions are sampled together, with less potential for bias towards the smouldering emissions. The burn took hold easily and plenty of smoke was sampled in the measurement path.

4.5 Alford's Point, hazard reduction burn

The Alford's Point burn occurred in somewhat unusual circumstances for a hazard reduction burn, with a strong breeze blowing towards the face of a steep escarpment, and the fire being first ignited near the top. The fire-fighters worked by igniting the fire in approximately 15 metre strips and allowing it to burn upwards towards a fire trail at the top, in front of a number of residential buildings. The spectrometer, telescope and retro-reflectors were set up ~ 42 m apart immediately leeward of the steep escarpment and away from any of the nearby homes. The strength of the wind was sufficient to push the flames towards the measurement path ensuring an excellent geometry to capture a good mixture of emissions representative of all states of burning occurring in the fire. This is illustrated in the photograph taken at the site shown in Fig. 3f.

New emission factors for Australian vegetation fires

C. Paton-Walsh et al.

Title Page

Abstract

Introduction

Conclusions

References

Tables

Figures

⏪

⏩

◀

▶

Back

Close

Full Screen / Esc

Printer-friendly Version

Interactive Discussion



Fanned by the wind, the fire burned well and the geometry of the measurement set-up resulted in very high mole fractions of trace gases being sampled in the measurement path. Despite personal protective equipment (goggles and masks), the smoke became too intense for us to stay with the spectrometer throughout the measurement period, however once set-up the open-path spectrometer ran autonomously and continued to record spectra through the thick smoke.

5 Results

5.1 Calculating emission factors for CO₂ and CO via the summation method

Emission factors for CO₂ and CO were calculated for all fires by summing the excess amounts of CO₂, CO, CH₄, C₂H₄, H₂CO, HCOOH and CH₃COOH from all spectra to yield total excess amounts Δ[CO₂], Δ[CO], Δ[CH₄], Δ[C₂H₄], Δ[H₂CO], Δ[HCOOH] and Δ[CH₃COOH] from each fire and applying Eqs. (1) and (2).

Thus the emission factor for CO₂ in g kg⁻¹ (assuming a carbon content “F_C” of 50 %) is given by Eq. (7):

$$EF_{CO_2} = 0.5 \times 1000 \times \frac{44}{12} \times \frac{\Delta[CO_2]}{\sum \left(\begin{array}{l} \Delta[CO_2] + \Delta[CO] + \Delta[CH_4] + 2\Delta[C_2H_4] \\ + \Delta[H_2CO] + \Delta[HCOOH] + 2\Delta[CH_3COOH] \end{array} \right)} \quad (7)$$

and the emission factor for CO in g kg⁻¹ (assuming a carbon content “F_C” of 50 %) is given by Eq. (8):

$$EF_{CO} = 0.5 \times 1000 \times \frac{28}{12} \times \frac{\Delta[CO]}{\sum \left(\begin{array}{l} \Delta[CO_2] + \Delta[CO] + \Delta[CH_4] + 2\Delta[C_2H_4] \\ + \Delta[H_2CO] + \Delta[HCOOH] + 2\Delta[CH_3COOH] \end{array} \right)} \quad (8)$$

This method produced modified combustion efficiencies that ranged from a minimum of 0.88 at the Lane Cove burn (with corresponding emission factors of 1583 g kg⁻¹ of

Title Page

Abstract

Introduction

Conclusions

References

Tables

Figures

◀

▶

◀

▶

Back

Close

Full Screen / Esc

Printer-friendly Version

Interactive Discussion



dry fuel consumed for CO₂ and 136 gkg⁻¹ for CO) to a maximum of 0.91 at the Abaroo Creek burn (with corresponding emission factors of 1647 gkg⁻¹ for CO₂ and 102 gkg⁻¹ for CO).

5.2 Uncertainties in emission factors for CO₂ and CO

5 An uncertainty budget was first calculated for $\Delta[\text{CO}_2]$ and $\Delta[\text{CO}]$ and then applied to the resulting emission factors calculated. The dominant uncertainty for both $\Delta[\text{CO}_2]$ and $\Delta[\text{CO}]$ is the assumed temperature, which causes both a spectral error (because the wrong line shape and line strengths are assumed in the fitting algorithm) and a density error, due to assuming the wrong air density when converting from the measured concentration in the line of path to mole fraction. The temperature was measured at
10 a single point close to the spectrometer but in reality the temperature may vary substantially across the spectrometer's line of sight with a significant probability of increased temperatures where there are enhanced amounts of trace gases absorbing such as in the flaming emissions from the fire. However, the increased temperatures are likely
15 to cover a small fraction of the whole path-length and so we estimated that the temperature error was unlikely to exceed 20 °C. (This is a conservative estimate, meant to account for the possibility that a large temperature error for a fraction of the path may be more significant than a smaller temperature error over the entire path). The resulting density error was calculated assuming ideal gas behaviour and the spectral errors were taken from the sensitivity studies undertaken by Smith et al. (2011). In
20 the case of CO₂ the density and spectral temperature errors are in the same direction giving a combined error of 15.3 % for an underestimation of the temperature of 20 °C, whereas for CO they partially compensate giving an overall temperature error of 5.1 %. These uncertainties are added in quadrature from those resulting from uncertainties
25 in the assumed background mole fractions, spectral fitting errors and errors in the HITRAN lines used in the retrieval. The resulting overall uncertainty estimates are 16.3 % for $\Delta[\text{CO}_2]$ and 6.3 % for $\Delta[\text{CO}]$, and the contributions are summarised in Table 3.

New emission factors for Australian vegetation fires

C. Paton-Walsh et al.

Title Page

Abstract

Introduction

Conclusions

References

Tables

Figures

◀

▶

◀

▶

Back

Close

Full Screen / Esc

Printer-friendly Version

Interactive Discussion



New emission factors for Australian vegetation fires

C. Paton-Walsh et al.

Title Page

Abstract

Introduction

Conclusions

References

Tables

Figures

◀

▶

◀

▶

Back

Close

Full Screen / Esc

Printer-friendly Version

Interactive Discussion



However, the resulting uncertainty in the emission factor calculated for CO_2 is very different because it depends upon the ratio C_i/C_T – i.e. the ratio of $\Delta[\text{CO}_2]$ to the sum of $\Delta[\text{CO}_2]$, $\Delta[\text{CO}]$, and the other carbon containing species. Since $\Delta[\text{CO}_2]$ is the dominant term in both the numerator and the denominator, uncertainties in this value are largely cancelled out, leaving an uncertainty in the ratio $C_{\text{CO}_2}/C_T \leq 1.5\%$. For CO , the opposite scenario is true because the uncertainties in $\Delta[\text{CO}_2]$ and $\Delta[\text{CO}]$ combine to produce an uncertainty in the ratio $C_{\text{CO}}/C_T \leq 12\%$.

Uncertainties in the molecular masses are vanishingly small but there is a large uncertainty in the carbon content of the fuel (F_C) which is not measured but taken to be 0.50 ± 0.05 . This value of 0.5 is the same as that used by Bennett et al. (2013), and our estimated uncertainties encompasses the value used by Volkova and Weston (2013) of 0.47 taken from the IPCC (2004) recommendation for trees and the mean values measured by Burling et al. (2010) of 0.51 ± 0.03 for fuels from southern USA. The carbon content of the fuel turns out to be the dominant uncertainty for calculating the emission factor for CO_2 and a major uncertainty in the emission factor for CO . The resulting overall uncertainty estimates are 10% for EF_{CO_2} and 16% for EF_{CO} , and the contributions are summarised in Table 4.

5.3 Calculating emission ratios to CO and CO_2

Emission factors for all other trace gases were calculated using the emission ratio to either CO or CO_2 , depending upon which showed the stronger correlation. Example correlation plots from the Alford's Point burn for gases that were most strongly correlated to CO_2 (C_2H_4 , H_2CO and N_2O) are shown in Fig. 4 along with the CO vs. CO_2 correlation plot.

All other gases (CH_4 , NH_3 , CH_3OH , CH_3COOH , HCOOH and C_2H_6 .) showed stronger correlation to CO , and example correlation plots from Alford's Point are shown in Fig. 5. CH_4 showed anomalous behaviour at Alford's Point (see Fig. 6) and for this reason CH_4 vs. CO from the Turrumurra burn is shown in Fig. 5. Emission ratios were derived from the gradients of these correlation plots using generalised least squares

regression. (This is the best fit to the points that minimises deviations from the line of fit in both x and y axes and is weighted by the uncertainties in both x and y .)

Uncertainties in the emission ratios are calculated from the relevant uncertainties in the gradient of the correlation plot of target gas and reference gas. The generalised least squares regression yields an uncertainty in the gradient but this value contains only random uncertainty and assumes that the uncertainties of each point are uncorrelated. Thus other factors that contribute to the uncertainty must also be considered. Table 5 shows the contributing factors to the uncertainties of the derived emission ratios, broken into contributions from the target gas (Δ_{gas}) and the reference gas (Δ_{ref}) – CO_2 or CO . Component values for the uncertainties arising from spectral temperature sensitivities are estimated by assuming a maximum 20°C temperature error and adding sensitivities of target gas and reference gas in quadrature. Relevant spectral sensitivities and uncertainties in the HITRAN database are taken from the literature where available (Paton-Walsh et al., 2005; Pinnock and Shine, 1998; Rothman et al., 2009; Smith et al., 2011). For CH_3COOH these values are not available and an estimated value of 10% is assigned to both the spectral temperature uncertainty and to the uncertainty in the library spectrum cross-sections (equivalent to a HITRAN error). Uncertainties in the derived gradients were taken from the generalised least squares regressions (using data from the fire that yielded the worst R^2 values – so as to provide a worst case scenario). The uncertainty in the gradient assumes that the uncertainties in the individual points are uncorrelated and hence it accounts for random uncertainties only. Thus the spectral fitting uncertainty estimated during the MALT fitting algorithm is also included because this is often not random but dominated by errors in the forward model.

Uncertainties in the reference gases (Δ_{ref}) were calculated using the components in Table 3 but excluding the uncertainties in background mole fractions and the error in density correction arising from temperature uncertainties. These components are excluded because the former does not contribute to the gradient and the latter cancels out as it produces the same error in the target gas and the reference gas. This yields

New emission factors for Australian vegetation fires

C. Paton-Walsh et al.

Title Page

Abstract

Introduction

Conclusions

References

Tables

Figures

◀

▶

◀

▶

Back

Close

Full Screen / Esc

Printer-friendly Version

Interactive Discussion



an uncertainty in Δ_{ref} of 10% for CO_2 and 3% for CO. Finally all uncertainties are added in quadrature to give a total uncertainty for each emission ratio.

Table 6 shows the results of the generalised least squares regression analysis, with the emission ratio and its uncertainty given. Also shown is the square of the correlation coefficient to a simple linear regression (R^2). This is also provided because it is a more commonly understood measure of the strength of the correlation.

Note that N_2O to CO_2 emission ratios could only be determined from Gulguer Nature Reserve and Alford's Point burns where spectra with very large enhancements of trace gases were measured (CO_2 in excess of 1000 ppm and CO in excess of 100 ppm). This is because N_2O sits under the CO and CO_2 bands and thus the emission ratio is difficult to measure unless the enhancements are very large. This is also true for C_2H_6 because its spectral absorption features are weak. Thus we only managed to determine a C_2H_6 to CO emission ratio for the Alford's Point burn.

5.4 Discussion of emission ratio results

Most trace gases exhibit very strong correlations with either CO or CO_2 , as can be seen by the large R^2 values given in Table 6. Also shown in Table 6 are the mean and standard deviation values for the emission ratios from all the fires sampled. For all gases, the natural variability (as seen in the standard deviation of emission ratios measured at different fires) exceeds the measurement uncertainty for the emission ratio at an individual fire.

There are two interesting anomalies in the correlation plots from the Alford's Point burn shown in Fig. 6. The first is a sudden flattening off of the CH_4 to CO gradient above 100 ppm of CO. The reason for this is not obvious, but we believe that it may be real, having checked for significant spectral artefacts. There is no sign of poor fits or saturation by either CH_4 or H_2O in the spectra, with transmission levels still at the 40–50% level. Excessive spectral temperature errors caused by really hot gases in the line of sight would probably not cause sufficient change in the CH_4 to CO ratios. Smith et al. (2010) showed that a 40°C underestimation of the temperature leads to ~ 8%

Title Page

Abstract

Introduction

Conclusions

References

Tables

Figures

◀

▶

◀

▶

Back

Close

Full Screen / Esc

Printer-friendly Version

Interactive Discussion



underestimation of the CH₄ mole fraction and ~ 4 % underestimation of the CO mole fraction (at 40 °C above room temperature). This equates to the CH₄ to CO emission ratio being underestimated by only ~ 1 % per 10 °C underestimation of the temperature. Whilst the effect is not necessarily linear, (so we cannot entirely rule out temperature errors as the cause), the magnitude of the effect is probably not enough to account for the differences that we see. There is no evidence of a similar effect in the Gulguer Nature Reserve results, which was the only other fire where CO enhancements in excess of 100 ppm were measured. The contrast in the CH₄ to CO correlation plots from Alford's Point and Gulguer Nature Reserve is illustrated in the upper panels of Fig. 6 where the points have been coloured by MCE. It appears that as the CH₄ to CO gradient lowers at higher CO values at Alford's Point, the MCE increases, (with mean MCE values for CO < 100 ppm of 0.84 and mean MCE for CO > 100 ppm of 0.91). This suggests the possibility that the change in emission ratio may be the result of different fuel burning as the fire reaches its most intense (e.g. eucalypt trees burning as well as understorey or larger woody fuels as opposed to smaller fine litter). Equally, it could be the same fuel burning but at a different fire intensity, leading to a different MCE.

The second anomaly is that the Alford's Point data display an unusually large NH₃ to CO gradient for spectra with CO enhancements above ~ 50 ppm (approximately twice that for spectra with CO enhancements below ~ 50 ppm). The spectra with lower enhancements have lower MCE and an NH₃ emission ratio typical of that measured at the other fires. Moreover, despite more scatter in the data, similar behaviour is evident in the Gulguer Nature Reserve data (see lower right panel of Fig. 6). The emission ratio for NH₃ to CO for low MCE at Gulguer is lower than for higher MCE values (see different colours in Fig. 6), again possibly indicative of different vegetation types contributing to the fire. None of the other fires resulted in spectra with enhancements large enough to confirm this behaviour. Alford's Point has the highest emission ratio for NH₃ to CO and Gulguer Nature Reserve the lowest of those measured in this study, providing further evidence of the very high natural variability of NH₃ emissions, which may be heavily dependent on the nitrogen content of the fuel burning.

New emission factors for Australian vegetation fires

C. Paton-Walsh et al.

[Title Page](#)[Abstract](#)[Introduction](#)[Conclusions](#)[References](#)[Tables](#)[Figures](#)[Back](#)[Close](#)[Full Screen / Esc](#)[Printer-friendly Version](#)[Interactive Discussion](#)

5.5 Comparison of emission ratios to previous studies

This study provides the first direct measurements of emission factors for many gases from Australian forest fires. In the absence of previous measurements of emission factors, it is interesting to compare our measured emission ratios with enhancement ratios (measured in aged smoke) from Australian forest fires reported in the literature.

Mean CH_3OH to CO ratios from this study (0.017 ± 0.006) are in excellent agreement with the only previous reported emission ratio from this ecosystem of 0.019 ± 0.001 using ground-based solar remote sensing Fourier transform spectrometry (Paton-Walsh et al., 2008). Mean NH_3 to CO and C_2H_6 to CO ratios from this study (0.023 ± 0.011) and (0.0037) respectively are higher than those reported by Paton-Walsh et al. (2005) (also using ground-based solar remote sensing Fourier transform spectrometry) of 0.0095 ± 0.0035 and 0.0023 ± 0.0005 . The discrepancy in NH_3 values is likely due to chemical loss in the aged smoke sampled in previous studies. Our single C_2H_6 to CO emission ratio is $\sim 30\%$ higher than the value reported by Paton-Walsh et al. (2005) but our estimated measurement uncertainty is 27% , and with only a single value it is difficult to know whether this is due to natural variability or measurement biases.

More surprising is the 10 times lower HCOOH to CO ratio measured in this study (0.0021 ± 0.0008) than the enhancement ratio measured by Paton-Walsh et al. (2005) of 0.021 ± 0.010 in smoke aged a few hours. Our emission ratio from this study is in much better agreement with Alvarado et al.'s (2011) measurement of 0.0031 ± 0.0021 for Canadian forest fires using the satellite-based sensor TES and Goode et al.'s (2000) measurement of 0.0031 ± 0.0009 for Canadian forest fires using airborne FTIR spectrometry. The larger value for enhancement ratios in aged smoke suggests that HCOOH may be chemically produced in the smoke plume as it ages. This is highly plausible since sunlight-induced oxidation of non-methane hydrocarbons is a major source of atmospheric HCOOH (Kavouras et al., 1998; Stavrou et al., 2012). The large excess amounts of hydrocarbons in the smoke plumes provide an excellent potential source of HCOOH . This theory is also supported by the large difference be-

New emission factors for Australian vegetation fires

C. Paton-Walsh et al.

Title Page

Abstract

Introduction

Conclusions

References

Tables

Figures



Back

Close

Full Screen / Esc

Printer-friendly Version

Interactive Discussion



tween the emission factor for HCOOH from extra-tropical fires estimated by Akagi et al. (2011) using only measurements in fresh smoke ($0.35 \pm 0.33 \text{ g kg}^{-1}$ dry fuel consumed) and that estimated by Andreae and Merlet (2001) using all available literature sources ($2.9 \pm 2.4 \text{ g kg}^{-1}$ dry fuel consumed). Our calculated emission factor for HCOOH of $0.4 \pm 0.2 \text{ g kg}^{-1}$ dry fuel consumed falls within the expected range for measurements made in fresh smoke and is also in good agreement with Akagi et al. (2013) measurement of $0.36 \pm 0.04 \text{ g kg}^{-1}$ for pine understory burns in South Carolina, USA measured by open-path FTIR spectrometry.

We may also compare the enhancement ratios with respect to CO for C_2H_4 and H_2CO reported by Paton-Walsh et al. (2005) and Young and Paton-Walsh (2011) from wildfires in Australian forests with our emission ratios with respect to CO_2 by assuming the mean emission factors for CO_2 and CO measured in this study. (This produces a multiplication factor of 0.114 to convert an emission ratio with respect to CO to an equivalent emission ratio with respect to CO_2). Thus the C_2H_4 to CO enhancement ratio reported by Paton-Walsh et al. (2005) of (0.0057 ± 0.0027) is equivalent to a C_2H_4 to CO_2 ratio of 0.00065 ± 0.00031 or approximately half our measured value of 0.0012 ± 0.0003 . Similarly, the H_2CO to CO enhancement ratios of 0.023 ± 0.007 and 0.016 ± 0.004 reported Paton-Walsh et al. (2005) and Young and Paton-Walsh (2011) respectively are equivalent to a H_2CO to CO_2 ratios of 0.0026 ± 0.0008 and 0.0018 ± 0.0005 , in broad agreement with our mean measured value of 0.0016 ± 0.0004 .

5.6 New emission factors for Australian temperate forest fires

Emission factors for CO_2 and CO were calculated by the summation method as described in Sect. 3.1 above. The results are shown in Table 7 for each individual fire along with the mean and standard deviation from all of the fires sampled. Emission factors for all other gases were calculated (via Eq. 5) from the CO_2 and CO emission factors for the relevant fires and the emission ratios in Table 6. The uncertainties were calculated by combining in quadrature the uncertainties in the emission ratios with the

New emission factors for Australian vegetation fires

C. Paton-Walsh et al.

Title Page

Abstract

Introduction

Conclusions

References

Tables

Figures

◀

▶

◀

▶

Back

Close

Full Screen / Esc

Printer-friendly Version

Interactive Discussion



uncertainty of the emission factor of the reference gas (CO or CO₂) as outlined in Table 1.

The results show that the standard deviation of the mean emission factor for CO₂ is significantly lower than the measurement uncertainties (which are dominated by the uncertainty assigned to assumed carbon content of the fuel). This suggests that the variability of the fuel carbon content in this ecosystem is less than the overall uncertainty assigned. For CO the emission factor uncertainty is dominated by uncertainty in the measurement of “ C_i/C_T ” – the fraction of carbon emitted as CO. The standard deviation of the mean CO emission factor is of a similar magnitude to the measurement uncertainty for individual fires, indicating no definitive evidence for variability above the measurement uncertainty. Since we have not included a term in the uncertainty budget to account for biases in the sampling – since it is so difficult to quantify – this suggests that we are measuring a true representative sample, or at least a consistent one. Further evidence for this comes from the small spread in MCE values from our five fires (0.88–0.91), despite significantly different measurement geometries. These MCE values are comparable to those calculated from the mean emission factors for CO₂ and CO presented by Akagi et al. (2011) for temperate forests of 0.92 and for extratropical forests of 0.89 (where extra-tropical forests represent a weighted average of boreal and temperate forests based on GFED3 biomass consumption estimates, van der Werf et al., 2010).

Mean MCE values reported for laboratory burns by Burling et al. (2010) are slightly higher at 0.93 ± 0.04 , suggesting that either the average literature values in Akagi et al. (2011) are biased towards smouldering combustion or that the laboratory fires are biased to flaming combustion. Both possibilities are plausible since laboratory fires lack the thermal mass to sustain smouldering combustion to the same degree as a real forest fire and the geometry of many ground-based measurements may bias the sampling towards smouldering combustion (as discussed previously).

Nevertheless the MCE values that we obtain lend confidence that open-path FTS methodology is a sound technique for measuring a representative sample as long as

**New emission factors
for Australian
vegetation fires**

C. Paton-Walsh et al.

Title Page

Abstract

Introduction

Conclusions

References

Tables

Figures



Back

Close

Full Screen / Esc

Printer-friendly Version

Interactive Discussion



However, our emission factor for CO is quite a bit higher and closer to their estimated mean value for extra-tropical forests of $122 \pm 44 \text{ g kg}^{-1}$ dry fuel consumed.

Also of note are higher emission factors for CH_3COOH and NH_3 (also more typical of extra-tropical forest estimates) and significantly lower C_2H_6 emissions as reported previously by Paton-Walsh et al. (2005).

6 Summary and conclusions

We present results from open-path FTIR measurements of emission factors for Australian temperate forest fires from five hazard reduction burns in New South Wales. A detailed description of the measurement set-up and analysis procedure is given, including recommended spectral regions for retrieving several trace gases from highly polluted smoky environments. Different methods for deriving best estimates for fire-averaged emission factors are presented and we conclude that, for our measurement geometry, it is best to use a whole fire integrated method (or “summation method”) to derive emission factors for CO_2 and CO. For all other trace gases, we recommend that the emission factor is derived using the emission ratio to one of these reference gases (CO_2 or CO), whichever gives the strongest correlation.

Detailed analysis of the uncertainty budget for these measurements reveals that the natural variability of the emission factor of CO_2 is substantially smaller than the overall measurement uncertainty (which is dominated by the uncertainty in the assumed carbon content of the fuel), suggesting that the true variability of the carbon content is smaller than the total uncertainty assigned. CO shows greater variability and for all other trace gases measured in this study the natural variability of the emissions is far greater than the measurement uncertainty for the emissions of any individual fire. Our study has insufficient statistics to determine likely causes of the variability and we therefore recommend that our mean emission factors be used in future biomass burning emissions inventories.

New emission factors for Australian vegetation fires

C. Paton-Walsh et al.

Title Page

Abstract

Introduction

Conclusions

References

Tables

Figures

◀

▶

◀

▶

Back

Close

Full Screen / Esc

Printer-friendly Version

Interactive Discussion



The recommended emission factors for Australian temperate forest fires (in grams of gas emitted per kilogram of dry fuel burned) are therefore:

1620 gkg⁻¹ of CO₂; 118 gkg⁻¹ of CO; 3.5 gkg⁻¹ of CH₄; 1.3 gkg⁻¹ of C₂H₄; 1.7 gkg⁻¹ of H₂CO; 2.4 gkg⁻¹ of CH₃OH; 3.8 gkg⁻¹ of CH₃COOH; 0.4 gkg⁻¹ of HCOOH; 1.7 gkg⁻¹ of NH₃; 0.15 gkg⁻¹ of N₂O and 0.5 gkg⁻¹ of C₂H₆.

Acknowledgements. The authors would like to acknowledge the invaluable assistance of the New South Wales Department of Environment, Climate Change and Water for enabling us to make measurements at their hazard reduction burns. Particular thanks are due to S. Evans, B. Sullivan, D. Menzies-Jackson, R. Clark and L. Tasker. Thanks are also due to B. Yokelson, I. Burling, M. Cameron and M. Wooster for their input to discussions on best choices for spectral windows and methods for estimating whole-fire emission factors. We are also grateful to those within the Centre for Atmospheric Chemistry at the University of Wollongong who have supported this work in many ways before, during and after the fires in particular D. Kubistin, G. Kettlewell, F. Phillips, T. Naylor, M. Riggenbach, and S. Wilson. Thanks are due to the Australian Research Council for funding this work as a small component of the Discovery Project DP110101948.

References

- Akagi, S. K., Yokelson, R. J., Wiedinmyer, C., Alvarado, M. J., Reid, J. S., Karl, T., Crouse, J. D., and Wennberg, P. O.: Emission factors for open and domestic biomass burning for use in atmospheric models, *Atmos. Chem. Phys.*, 11, 4039–4072, doi:10.5194/acp-11-4039-2011, 2011.
- Akagi, S. K., Burling, I. R., Mendoza, A., Johnson, T. J., Cameron, M., Griffith, D. W. T., Paton-Walsh, C., Weise, D. R., Reardon, J., and Yokelson, R. J.: Field measurements of trace gases emitted by prescribed fires in southeastern US pine forests using an open-path FTIR system, *Atmos. Chem. Phys.*, 14, 199–215, doi:10.5194/acp-14-199-2014, 2014.
- Alvarado, M. J., Cady-Pereira, K. E., Xiao, Y. P., Millet, D. B., and Payne, V. H.: Emission ratios for ammonia and formic acid and observations of Peroxy Acetyl Nitrate (PAN) and ethylene in biomass burning smoke as seen by the Tropospheric Emission Spectrometer (TES), *Atmosphere*, 2, 633–654, 2011.

New emission factors for Australian vegetation fires

C. Paton-Walsh et al.

Title Page

Abstract

Introduction

Conclusions

References

Tables

Figures



Back

Close

Full Screen / Esc

Printer-friendly Version

Interactive Discussion



New emission factors for Australian vegetation fires

C. Paton-Walsh et al.

Title Page

Abstract

Introduction

Conclusions

References

Tables

Figures

◀

▶

◀

▶

Back

Close

Full Screen / Esc

Printer-friendly Version

Interactive Discussion



- Andreae, M. O. and Merlet, P.: Emission of trace gases and aerosols from biomass burning, *Global Biogeochem. Cy.*, 15, 955–966, 2001.
- Australian-Greenhouse-Office: National greenhouse gas inventory 2004, Rep., Australian Government Department of the Environment and Heritage, Australia, 2006.
- 5 Bacsik, Z., Mink, J., and Keresztury, G.: FTIR spectroscopy of the atmosphere. I. Principles and methods, *Appl. Spectrosc. Rev.*, 39, 295–363, 2004.
- Bennett, L. T., Aponte, C., Tolhurst, K. G., Löw, M., and Baker, T. G.: Decreases in standing tree-based carbon stocks associated with repeated prescribed fires in a temperate mixed-species eucalypt forest, *Forest Ecol. Manag.*, 306, 243–255, 2013.
- 10 Burling, I. R., Yokelson, R. J., Griffith, D. W. T., Johnson, T. J., Veres, P., Roberts, J. M., Warneke, C., Urbanski, S. P., Reardon, J., Weise, D. R., Hao, W. M., and de Gouw, J.: Laboratory measurements of trace gas emissions from biomass burning of fuel types from the southeastern and southwestern United States, *Atmos. Chem. Phys.*, 10, 11115–11130, doi:10.5194/acp-10-11115-2010, 2010.
- 15 Cottrill, D. A.: Seasonal climate summary Southern Hemisphere (spring 2011): La Nina returns, *Aust. Meteorol. Oceanogr. J.*, 62, 179–192, 2012.
- Giglio, L., Loboda, T., Roy, D. P., Quayle, B., and Justice, C. O.: An active-fire based burned area mapping algorithm for the MODIS sensor, *Remote Sens. Environ.*, 113, 408–420, 2009.
- Giglio, L., Randerson, J. T., and Van Der Werf, G. R.: Analysis of daily, monthly, and annual burned area using the fourth-generation global fire emissions database (GFED4), *J. Geophys. Res.-Biogeo.*, 118, 317–328, 2013.
- 20 Glatthor, N., Höpfner, M., Semeniuk, K., Lupu, A., Palmer, P. I., McConnell, J. C., Kaminski, J. W., von Clarmann, T., Stiller, G. P., Funke, B., Kellmann, S., Linden, A., and Wiegeler, A.: The Australian bushfires of February 2009: MIPAS observations and GEM-AQ model results, *Atmos. Chem. Phys.*, 13, 1637–1658, doi:10.5194/acp-13-1637-2013, 2013.
- 25 Goode, J. G., Yokelson, R. J., Susott, R. A., and Ward, D. E.: Trace gas emissions from laboratory biomass fires measured by open-path Fourier transform infrared spectroscopy: fires in grass and surface fuels, *J. Geophys. Res.-Atmos.*, 104, 21237–21245, 1999.
- 30 Goode, J. G., Yokelson, R. J., Ward, D. E., Susott, R. A., Babbitt, R. E., Davies, M. A., and Hao, W. M.: Measurements of excess O₃, CO₂, CO, CH₄, C₂H₄, C₂H₂, HCN, NO, NH₃, HCOOH, CH₃COOH, HCHO, and CH₃OH in 1997 Alaskan biomass burning plumes by airborne Fourier transform infrared spectroscopy (AFTIR), *J. Geophys. Res.*, 105, 30109–30125, 2000.

New emission factors for Australian vegetation fires

C. Paton-Walsh et al.

Title Page

Abstract

Introduction

Conclusions

References

Tables

Figures

◀

▶

◀

▶

Back

Close

Full Screen / Esc

Printer-friendly Version

Interactive Discussion

- Griffith, D. W. T.: Synthetic calibration and quantitative analysis of gas-phase FT-IR spectra, *Appl. Spectrosc.*, 50, 59–70, 1996.
- Griffith, D. W. T., Mankin, W. G., Coffey, M. T., Ward, D. E., and Riebau, A.: FTIR Remote Sensing of Biomass Burning Emissions of CO₂, CO, CH₄, CH₂O, NO, NO₂, NH₃ and N₂O, in *Global Biomass Burning: Atmospheric, Climatic and Biospheric Implications*, edited by: Levine, J. S., MIT Press, Cambridge, 230–239, 1991.
- Griffith, D. W. T., Deutscher, N. M., Caldow, C., Kettlewell, G., Riggensbach, M., and Hammer, S.: A Fourier transform infrared trace gas and isotope analyser for atmospheric applications, *Atmos. Meas. Tech.*, 5, 2481–2498, doi:10.5194/amt-5-2481-2012, 2012.
- Guérette, É.-A. and Paton-Walsh, C.: New emission factors for Australian temperate forest fires: measurements by SIFT-MS and FTIR, *Atmos. Chem. Phys.*, in preparation, 2014.
- Hao, W. M. and Ward, D. E.: Methane production from global biomass burning, *J. Geophys. Res.-Atmos.*, 98, 20657–20661, 1993.
- Haverd, V., Raupach, M. R., Briggs, P. R., Canadell, J. G., Davis, S. J., Law, R. M., Meyer, C. P., Peters, G. P., Pickett-Heaps, C., and Sherman, B.: The Australian terrestrial carbon budget, *Biogeosciences*, 10, 851–869, doi:10.5194/bg-10-851-2013, 2013.
- Hurst, D. F., Griffith, D. W. T., and Cook, G. D.: Trace gas emissions from biomass burning in tropical Australian savannas, *J. Geophys. Res.-Atmos.*, 99, 16441–16456, 1994a.
- Hurst, D. F., Griffith, D. W. T., Carras, J. N., Williams, D. J., and P. J. Fraser: Measurements of trace gases emitted by Australian savanna fires during the 1990 dry season, *J. Atmos. Chem.*, 18, 33–56, 1994b.
- Hurst, D. F., Griffith, D. W. T., and Cook, G. D.: Trace-gas emissions from biomass burning in Australia, in: *Biomass Burning and Global Change*, edited by: Levine, J. S., The MIT Press, London, England, 787–792, 1996.
- IPCC: Good practice guidance for land use, land-use change and forestry (GPGGLULUCF), Chapter 3. IPCC Report, 2004: available at: <http://www.ipcc-nggip.iges.or.jp/public/gpglulucf/gpglulucf.html> (last access: 11 November 2013), 2004.
- Ito, A. and Penner, J. E.: Global estimates of biomass burning emissions based on satellite imagery for the year 2000, *J. Geophys. Res.*, 109, D14S05, doi:10.1029/2003JD004423, 2004.
- Kavouras, I. G., Mihalopoulos, N., and Stephanou, E. G.: Formation of atmospheric particles from organic acids produced by forests, *Nature*, 395, 683–686, 1998.

**New emission factors
for Australian
vegetation fires**

C. Paton-Walsh et al.

Title Page

Abstract

Introduction

Conclusions

References

Tables

Figures

◀

▶

◀

▶

Back

Close

Full Screen / Esc

Printer-friendly Version

Interactive Discussion



- Lobert, J. M. and Scharffe, D. H.: Experimental evaluation of biomass burning emissions, in: *Global Biomass Burning: Atmospheric, Climatic, and Biospheric Implications*, edited by: Levine, J. S., MIT Press, Cambridge, 289–304, 1991.
- Maleknia, S. D., Bell, T. L., and Adams, M. A.: Eucalypt smoke and wildfires: temperature dependent emissions of biogenic volatile organic compounds, *Int. J. Mass Spectrom.*, 279, 126–133, 2009.
- Meyer, C. P., Cook, G. D., Reisen, F., Smith, T. E. L., Tattaris, M., Russell-Smith, J., Maier, S. W., Yates, C. P., and Wooster, M. J.: Direct measurements of the seasonality of emission factors from savanna fires in northern Australia, *J. Geophys. Res.-Atmos.*, 117, D20305, doi:10.1029/2012JD017671, 2012.
- Pak, B. C., Langenfelds, R. L., Young, S. A., Francey, R. J., Meyer, C. P., Kivlighon, L. M., Cooper, L. N., Dunse, B. L., Allison, C. E., Steele, L. P., Galbally, I. E., and Weeks, I. A.: Measurements of biomass burning influences in the troposphere over southeast Australia during the SAFARI 2000 dry season campaign, *J. Geophys. Res.-Atmos.*, 108, 8480, doi:10.1029/2002JD002343, 2003.
- Paton-Walsh, C., Jones, N., Wilson, S., Meier, A., Deutscher, N., Griffith, D., Mitchell, R., and Campbell, S.: Trace gas emissions from biomass burning inferred from aerosol optical depth, *Geophys. Res. Lett.*, 31, L05116, doi:10.1029/2003gl018973, 2004.
- Paton-Walsh, C., Jones, N. B., Wilson, S. R., Haverd, V., Meier, A., Griffith, D. W. T., and Rinsland, C. P.: Measurements of trace gas emissions from Australian forest fires and correlations with coincident measurements of aerosol optical depth, *J. Geophys. Res.-Atmos.*, 110, D24305, doi:10.1029/2005jd006202, 2005.
- Paton-Walsh, C., Wilson, S. R., Jones, N. B., and Griffith, D. W. T.: Measurement of methanol emissions from Australian wildfires by ground-based solar Fourier transform spectroscopy, *Geophys. Res. Lett.*, 35, L08810, doi:10.1029/2007gl032951, 2008.
- Paton-Walsh, C., Emmons, L. K., and Wilson, S. R.: Estimated total emissions of trace gases from the Canberra Wildfires of 2003: a new method using satellite measurements of aerosol optical depth & the MOZART chemical transport model, *Atmos. Chem. Phys.*, 10, 5739–5748, doi:10.5194/acp-10-5739-2010, 2010a.
- Paton-Walsh, C., Deutscher, N. M., Griffith, D. W. T., Forgan, B. W., Wilson, S. R., Jones, N. B., and Edwards, D. P.: Trace gas emissions from savanna fires in northern Australia, *J. Geophys. Res.-Atmos.*, 115, D16314, doi:10.1029/2009jd013309, 2010b.

New emission factors for Australian vegetation fires

C. Paton-Walsh et al.

Title Page

Abstract

Introduction

Conclusions

References

Tables

Figures

◀

▶

◀

▶

Back

Close

Full Screen / Esc

Printer-friendly Version

Interactive Discussion



Paton-Walsh, C., Emmons, L. K., and Wiedinmyer, C.: Australia's Black Saturday fires – comparison of techniques for estimating emissions from vegetation fires, *Atmos. Environ.*, **60**, 262–270, 2012.

Pfister, G., Hess, P. G., Emmons, L. K., Lamarque, J. F., Wiedinmyer, C., Edwards, D. P., Petron, G., Gille, J. C., and Sachse, G. W.: Quantifying CO emissions from the 2004 Alaskan wildfires using MOPITT CO data, *Geophys. Res. Lett.*, **32**, L11809, doi:10.1029/2005gl022995, 2005.

Phillips, F. A., Bai, M., Naylor, T., Bryan, G. R., Tonini, M., Jones, F. M., Malano, G., Pinares-Patino, C. S., and Griffith, D. W. T.: Methane emissions from a range of livestock management systems, estimated using the open-path FTIR Spectroscopy, paper presented at 4th International Conference on Greenhouse Gases and Animal Agriculture, edited by: Mc Geough, E. J. and McGinn, S. M., Banff, AB, Canada, 3–8 October 2011, p. 145, 2011.

Pinnock, S. and Shine, K. P.: The effects of changes in HITRAN and uncertainties in the spectroscopy on infrared irradiance calculations, *J. Atmos. Sci.*, **55**, 1950–1964, 1998.

Reisen, F. and Brown, S. K.: Australian firefighters' exposure to air toxics during bushfire burns of autumn 2005 and 2006, *Environ. Int.*, **35**, 342–352, 2009.

Reisen, F., Meyer, C. P., McCaw, L., Powell, J. C., Tolhurst, K., Keywood, M. D., and Gras, J. L.: Impact of smoke from biomass burning on air quality in rural communities in southern Australia, *Atmos. Environ.*, **45**, 3944–3953, 2011.

Rothman, L. S., Gordon, I. E., Barbe, A., Benner, D. C., Bernath, P. E., Birk, M., Boudon, V., Brown, L. R., Campargue, A., Champion, J. P., Chance, K., Coudert, L. H., Dana, V., Devi, V. M., Fally, S., Flaud, J. M., Gamache, R. R., Goldman, A., Jacquemart, D., Kleiner, I., Lacome, N., Lafferty, W. J., Mandin, J. Y., Massie, S. T., Mikhailenko, S. N., Miller, C. E., Moazzen-Ahmadi, N., Naumenko, O. V., Nikitin, A. V., Orphal, J., Perevalov, V. I., Perrin, A., Predoi-Cross, A., Rinsland, C. P., Rotger, M., Simeckova, M., Smith, M. A. H., Sung, K., Tashkun, S. A., Tennyson, J., Toth, R. A., Vandaele, A. C., and Vander Auwera, J.: The HITRAN 2008 molecular spectroscopic database, *J. Quant. Spectrosc. Ra.*, **110**, 533–572, 2009.

Seiler, W. and Crutzen, P. J.: Estimates of gross and net fluxes of carbon between the biosphere and atmosphere, *Climatic Change*, **2**, 207–247, 1980.

Sharpe, S. W., Johnson, T. J., Sams, R. L., Chu, P. M., Rhoderick, G. C., and Johnson, P. A.: Gas-phase databases for quantitative infrared spectroscopy, *Appl. Spectrosc.*, **58**, 1452–1461, 2004.

New emission factors for Australian vegetation fires

C. Paton-Walsh et al.

Title Page

Abstract

Introduction

Conclusions

References

Tables

Figures

◀

▶

◀

▶

Back

Close

Full Screen / Esc

Printer-friendly Version

Interactive Discussion



Shirai, T., Blake, D. R., Meinardi, S., Rowland, F. S., Russell-Smith, J., Edwards, A., Kondo, Y., Koike, M., Kita, K., Machida, T., Takegawa, N., Nishi, N., Kawakami, S., and Ogawa, T.: Emission estimates of selected volatile organic compounds from tropical savanna burning in northern Australia, *J. Geophys. Res.*, 108, BIB 10-1–BIB 10-14, 2003.

5 Smith, T. E. L., Wooster, M. J., Tattaris, M., and Griffith, D. W. T.: Absolute accuracy and sensitivity analysis of OP-FTIR retrievals of CO₂, CH₄ and CO over concentrations representative of “clean air” and “polluted plumes”, *Atmos. Meas. Tech.*, 4, 97–116, doi:10.5194/amt-4-97-2011, 2011.

10 Smith, T. E. L., Paton-Walsh, C., Meyer, C. P., Cook, G. D., Maier, S. W., Yates, C. P., and Wooster, M. J.: New emission factors for Australian vegetation fires measured using open-path Fourier transform infrared spectroscopy – Part 2: Australian tropical savanna fires, *Atmos. Chem. Phys. Discuss.*, in review, 2014.

15 Stavrakou, T., Muller, J. F., Peeters, J., Razavi, A., Clarisse, L., Clerbaux, C., Coheur, P. F., Hurtmans, D., De Maziere, M., Vigouroux, C., Deutscher, N. M., Griffith, D. W. T., Jones, N., and Paton-Walsh, C.: Satellite evidence for a large source of formic acid from boreal and tropical forests, *Nat. Geosci.*, 5, 26–30, 2012.

Tobin, S. and Skinner, T. C. L.: Seasonal climate summary Southern Hemisphere (autumn 2011): one of the strongest La Nina events on record begins to decline, *Aust. Meteorol. Oceanogr. J.*, 62, 39–50, 2012.

20 van der Werf, G. R., Randerson, J. T., Giglio, L., Collatz, G. J., Kasibhatla, P. S., and Arellano Jr., A. F.: Interannual variability in global biomass burning emissions from 1997 to 2004, *Atmos. Chem. Phys.*, 6, 3423–3441, doi:10.5194/acp-6-3423-2006, 2006.

25 van der Werf, G. R., Randerson, J. T., Giglio, L., Collatz, G. J., Mu, M., Kasibhatla, P. S., Morton, D. C., DeFries, R. S., Jin, Y., and van Leeuwen, T. T.: Global fire emissions and the contribution of deforestation, savanna, forest, agricultural, and peat fires (1997–2009), *Atmos. Chem. Phys.*, 10, 11707–11735, doi:10.5194/acp-10-11707-2010, 2010.

Volkova, L. and Weston, C.: Redistribution and emission of forest carbon by planned burning in *Eucalyptus obliqua* (L. Herit.) forest of south-eastern Australia, *Forest Ecol. Manag.*, 304, 383–390, 2013.

30 Ward, D. E. and Radke, L. F.: Emissions measurements from vegetation fires: a comparative evaluation of methods and results, in: *Fire in the Environment: The Ecological, Atmospheric and Climatic Importance of Vegetation Fires*, edited by: Crutzen, P. J. and Goldammer, J. G., 53–76, 1993.

New emission factors for Australian vegetation fires

C. Paton-Walsh et al.

Title Page

Abstract

Introduction

Conclusions

References

Tables

Figures

◀

▶

◀

▶

Back

Close

Full Screen / Esc

Printer-friendly Version

Interactive Discussion

Wiedinmyer, C., Akagi, S. K., Yokelson, R. J., Emmons, L. K., Al-Saadi, J. A., Orlando, J. J., and Soja, A. J.: The Fire INventory from NCAR (FINN): a high resolution global model to estimate the emissions from open burning, *Geosci. Model Dev.*, 4, 625–641, doi:10.5194/gmd-4-625-2011, 2011.

5 Wooster, M. J., Zhukov, B., and Oertel, D.: Fire radiative energy for quantitative study of biomass burning: derivation from the BIRD experimental satellite and comparison to MODIS fire products, *Remote Sens. Environ.*, 86, 83–107, 2003.

Wooster, M. J., Roberts, G., Perry, G. L. W., and Kaufman, Y. J.: Retrieval of biomass combustion rates and totals from fire radiative power observations: FRP derivation and calibration relationships between biomass consumption and fire radiative energy release, *J. Geophys. Res.-Atmos.*, 110, D24311, 10.1029/2005jd006318, 2005.

10 Wooster, M. J., Freeborn, P. H., Archibald, S., Oppenheimer, C., Roberts, G. J., Smith, T. E. L., Govender, N., Burton, M., and Palumbo, I.: Field determination of biomass burning emission ratios and factors via open-path FTIR spectroscopy and fire radiative power assessment: headfire, backfire and residual smouldering combustion in African savannahs, *Atmos. Chem. Phys.*, 11, 11591–11615, doi:10.5194/acp-11-11591-2011, 2011.

Yokelson, R. J., Griffith, D. W. T., and Ward, D. E.: Open-path Fourier transform infrared studies of large-scale laboratory biomass fires, *J. Geophys. Res.*, 101, 21067–21080, 1996.

Yokelson, R. J., Susott, R., Ward, D. E., Reardon, J., and Griffith, D. W. T.: Emissions from smoldering combustion of biomass measured by open-path Fourier transform infrared spectroscopy, *J. Geophys. Res.*, 102, 18865–18877, doi:10.1029/97jd00852, 1997.

20 Yokelson, R. J., Goode, J. G., Ward, D. E., Susott, R. A., Babbitt, R. E., Wade, D. D., Bertschi, I., Griffith, D. W. T., and Hao, W. M.: Emissions of formaldehyde, acetic acid, methanol, and other trace gases from biomass fires in North Carolina measured by airborne Fourier transform infrared spectroscopy, *J. Geophys. Res.*, 104, 30109–30125, 1999a.

Yokelson, R. J., Goode, J. G., Ward, D. E., Susott, R. A., Babbitt, R. E., Wade, D. D., Bertschi, I., Griffith, D. W. T., and Hao, W. M.: Emissions of formaldehyde, acetic acid, methanol, and other trace gases from biomass fires in North Carolina measured by airborne Fourier transform infrared spectroscopy, *J. Geophys. Res.-Atmos.*, 104, 30109–30125, 1999b.

30 Yokelson, R. J., Karl, T., Artaxo, P., Blake, D. R., Christian, T. J., Griffith, D. W. T., Guenther, A., and Hao, W. M.: The Tropical Forest and Fire Emissions Experiment: overview and airborne fire emission factor measurements, *Atmos. Chem. Phys.*, 7, 5175–5196, doi:10.5194/acp-7-5175-2007, 2007.

Young, E. and Paton-Walsh, C.: Emission ratios of the tropospheric ozone precursors nitrogen dioxide and formaldehyde from Australia's black saturday fires, Atmosphere, 2, 617–632, 2011.

**New emission factors
for Australian
vegetation fires**

C. Paton-Walsh et al.

Title Page

Abstract

Introduction

Conclusions

References

Tables

Figures



Back

Close

Full Screen / Esc

Printer-friendly Version

Interactive Discussion



New emission factors for Australian vegetation fires

C. Paton-Walsh et al.

Table 1. Spectral regions used for trace gas retrievals and trace gas species fitted.

Trace Gas(es) of interest	Interfering species fitted	Spectral region fitted (cm ⁻¹)	Fit to continuum level	Instrument line shape
CO and CO ₂ (and N ₂ O) ^a	H ₂ O	2080–2270	2nd order polynomial	fit phase and eff. apodisation
CH ₄	H ₂ O	2980–3105	2nd order polynomial	fit phase and eff. apodisation
C ₂ H ₄ and NH ₃	H ₂ O	920–1000	2nd order polynomial	fit phase and eff. apodisation
H ₂ CO	H ₂ O	2730–2800	2nd order polynomial	fit phase, fix eff. apodisation
CH ₃ OH	H ₂ O, NH ₃ ,	1020–1055	2nd order polynomial	fit phase, fix eff. apodisation
HCOOH	H ₂ O, NH ₃ ,	1060–1150	2nd order polynomial	fit phase and eff. apodisation
CH ₃ COOH ^b	H ₂ O, NH ₃ , HCOOH	1130–1230	Slope only (1st order)	fit phase and eff. apodisation
C ₂ H ₆ ^c	H ₂ O, CH ₄ , C ₂ H ₄	2971–3002	2nd order polynomial	fit phase, fix eff. apodisation
C ₂ H ₂ and HCN ^d	H ₂ O, CO ₂ ,	710–760	2nd order polynomial	fit phase, fix eff. apodisation

a Accurate N₂O retrievals are difficult as the features lie under the stronger bands of CO and ¹³CO₂.

b Uses a library spectrum as HITRAN lines are not available.

c C₂H₆ features are very weak and can only be retrieved accurately at higher concentrations than were usual at these burns.

d C₂H₂ and HCN – this window was used for spectra recorded with the bi-static instrumentation used at the savanna burns only. The mono-static instrumentation described in this paper used a detector with insufficient sensitivity at these longer wavelengths for this retrieval.

[Title Page](#)
[Abstract](#)
[Introduction](#)
[Conclusions](#)
[References](#)
[Tables](#)
[Figures](#)
[Back](#)
[Close](#)
[Full Screen / Esc](#)
[Printer-friendly Version](#)
[Interactive Discussion](#)


New emission factors for Australian vegetation fires

C. Paton-Walsh et al.

Table 2. Summary of hazard reduction burns where measurements were made including location, date, vegetation type, burned area, fuel loading before burn along with the hours of burning sampled, the total number of fire-influenced spectra collected and the peak mole fractions of CO₂ and CO measured.

Fire name, location and (latitude and longitude)	Date	Vegetation/Fuel description	Area burned (ha)	Fuel loading (tha ⁻¹)	Number of fire spectra	Hours of burning sampled ^b	Peak path-averaged CO ₂ and CO measured
Max Allen Drive, Lane Cove National Park, NSW, (33.79° S, 151.15° E)	31 Aug 2010	Dry sclerophyll open woodland	4.8	18–26	270	2 h, 31 min	~ 800 ppm CO ₂ ~ 30 ppm CO
Gibberagong, North Turrumurra, Ku-Ring-Gai Chase National Park, NSW, (33.67° S, 151.15° E)	28 Sep 2010	Banksia/Hakea heath and Sclerophyll shrub forest	148.5	20–25	232	2 h, 6 min	~ 900 ppm CO ₂ ~ 55 ppm CO
Abaroo Creek, Heathcote National Park, NSW: North end (34.10° S, 150.99° E) and South end: (34.13° S, 150.99° E)	11 May 2012 and 12 May 2012	Shrubby dry sclerophyll forest/heathland	115 ^a	12.5	344 and 278	2 h, 3 min and 2 h, 22 min	~ 800 ppm CO ₂ ~ 40 ppm CO
Gulguer Nature Reserve, NSW, (33.95° S, 150.62° E)	16 May 2012	Open eucalypt woodland forest with grassy understorey	32	8–10	333	2 h, 6 min	~ 2200 ppm CO ₂ ~ 140 ppm CO
Alford's Point, Georges River National Park, NSW, (33.99° S, 151.02° E)	23 May 2012	Shrubby dry sclerophyll forest	18	14–18	496	3 h, 6 min	~ 3400 ppm CO ₂ ~ 180 ppm CO

^aTotal area burned in Heathcote National Park, NSW, over the two days.

^bHours of burning sampled is the difference between the time that the first and last smoke-affected spectra were recorded. In some cases spectra were lost during this time due to fire trucks or fire fighters obscuring the measurement path or excluded due to insufficient enhancements over background values.

[Title Page](#)
[Abstract](#)
[Introduction](#)
[Conclusions](#)
[References](#)
[Tables](#)
[Figures](#)
[Back](#)
[Close](#)
[Full Screen / Esc](#)
[Printer-friendly Version](#)
[Interactive Discussion](#)


New emission factors for Australian vegetation fires

C. Paton-Walsh et al.

Title Page

Abstract

Introduction

Conclusions

References

Tables

Figures

⏪

⏩

◀

▶

Back

Close

Full Screen / Esc

Printer-friendly Version

Interactive Discussion



Table 3. Totals and component values of the uncertainty budget for calculating $\Delta[\text{CO}_2]$ and $\Delta[\text{CO}]$.

Gas	Background mole fraction	Temperature error (spectral)	Temperature error (density)	Spectral fitting error	HITRAN error	Summed in quadrature
ΔCO_2	2.5%	+8.6%	+6.7%	1%	5%	16.3%
ΔCO	2.5%	−1.6%	+6.7%	2%	2%	6.3%

New emission factors for Australian vegetation fires

C. Paton-Walsh et al.

Title Page

Abstract

Introduction

Conclusions

References

Tables

Figures

◀

▶

◀

▶

Back

Close

Full Screen / Esc

Printer-friendly Version

Interactive Discussion



Table 4. Totals and component values of the uncertainty budget for calculating EF_{CO_2} and EF_{CO} .

	Uncertainty in C_i/C_T	Uncertainty in F_C	Summed in Quadrature
EF_{CO_2}	1.5 %	10 %	10 %
EF_{CO}	12 %	10 %	16 %

New emission factors for Australian vegetation fires

C. Paton-Walsh et al.

Title Page

Abstract

Introduction

Conclusions

References

Tables

Figures

◀

▶

◀

▶

Back

Close

Full Screen / Esc

Printer-friendly Version

Interactive Discussion



Table 5. Totals and component values of the uncertainty budget for calculating emission ratios.

Emission ratio	Temperature uncertainty (spectral) for 20 °C	Spectral fitting uncertainty	HITRAN uncertainty	Uncertainty in gradient	Δ gas total uncertainty	Δ ref Total uncertainty	Total emission ratio uncertainty
C ₂ H ₄ /CO ₂	12%	5%	5%	1%	14%	10%	17%
H ₂ CO/CO ₂	6.4%	5%	5%	1.4%	10%	10%	14%
N ₂ O/CO ₂	5%	4%	5%	5%	10%	10%	14%
CH ₄ /CO	4.4%	2%	5%	0.8%	7%	3%	8%
CH ₃ OH/CO	4.4%	6%	5%	0.8%	9%	3%	9%
CH ₃ COOH/CO	10%*	3%	10%*	0.6%	14%	3%	15%
NH ₃ /CO	10.8%	2%	5%	0.5%	12%	3%	12%
HCOOH/CO	8%	16%	5%	5.4%	19%	3%	20%
C ₂ H ₆ /CO	9.2%	25%	5%	2.6%	27%	3%	27%

* For CH₃COOH values for the spectral temperature sensitivity and the HITRAN uncertainty and are not available or not relevant and instead an estimated value of 10% is assigned to both the spectral temperature uncertainty and to the uncertainty in the library spectrum cross-sections (equivalent to a HITRAN error) so that an estimate may be obtained for the overall emission ratio uncertainty.

New emission factors for Australian vegetation fires

C. Paton-Walsh et al.

Table 6. Shows the results of the generalised least squares regression analysis, with the emission ratio (ER) and its uncertainty (S_{ER}) given. Also shown is “ R^2 ” the square of the correlation coefficient to a simple linear regression. The arithmetic mean and standard deviation of the emission ratios measured at all of the fires are given. In addition the modified combustion efficiency (MCE) values calculated via the summation method for each fire are given.

	Lane Cove	R^2	Turramurra	R^2	Abaroo Creek	R^2	Gulguer	R^2	Alford's Point	R^2	Mean	StdDev
C_2H_4/CO_2	0.0016 ± 0.0003	0.83	0.0010 ± 0.0002	0.96	0.0010 ± 0.0002	0.97	0.0010 ± 0.0002	0.95	0.0015 ± 0.0003	0.98	0.0012	0.0003
H_2CO/CO_2	0.0022 ± 0.0003	0.73	0.0013 ± 0.0002	0.89	0.0012 ± 0.0002	0.90	0.0015 ± 0.0002	0.91	0.0016 ± 0.0002	0.98	0.0016	0.0004
N_2O/CO_2							0.00013 ± 0.00002	0.81	0.000054 ± 0.000008	0.87	0.00009	0.00005
CH_4/CO	0.062 ± 0.005	0.91	0.048 ± 0.004	0.98	0.046 ± 0.003	0.98	0.041 ± 0.003	0.98	0.059 ± 0.004	0.92	0.051	0.009
CH_3OH/CO	0.026 ± 0.002	0.90	0.013 ± 0.001	0.95	0.013 ± 0.001	0.93	0.012 ± 0.001	0.94	0.021 ± 0.002	0.97	0.017	0.006
CH_3COOH/CO	0.019 ± 0.003	0.86	0.012 ± 0.002	0.85	0.012 ± 0.002	0.97	0.015 ± 0.002	0.93	0.017 ± 0.002	0.98	0.015	0.003
NH_3/CO	0.026 ± 0.004	0.90	0.015 ± 0.002	0.85	0.023 ± 0.003	0.93	0.012 ± 0.002	0.91	0.039 ± 0.010 *	0.96	0.023	0.011
$HCOOH/CO$	0.0033 ± 0.0006	0.80	0.0015 ± 0.0003	0.69	0.0017 ± 0.0003	0.88	0.0020 ± 0.0004	0.92	0.0020 ± 0.0004	0.96	0.0021	0.0007
C_2H_6/CO									0.0037 ± 0.0010	0.81	(0.0037)	
MCE	0.88		0.91		0.91		0.90		0.88			

* Alford's Point NH_3 vs. CO shows anomalous behaviour above ~ 50 ppm of CO, with much larger NH_3 to CO emission ratio than for any other burn. Since the emission ratio changes with MCE in the burn (see Fig. 6) a larger uncertainty has been assigned for this emission ratio.

[Title Page](#)
[Abstract](#)
[Introduction](#)
[Conclusions](#)
[References](#)
[Tables](#)
[Figures](#)
[Back](#)
[Close](#)
[Full Screen / Esc](#)
[Printer-friendly Version](#)
[Interactive Discussion](#)


New emission factors for Australian vegetation fires

C. Paton-Walsh et al.

Table 7. Emission factors (EF_{gas}) in g kg^{-1} and uncertainties for each fire along with the mean and standard deviation of the emission factors from all of the fires sampled.

	Lane Cove	Turrumurra	Abaroo Creek	Gulguer Nature	Alford's Point Reserve	Mean and (Std Dev) from this study	Akagi et al. (2011) for temperate forests	Akagi et al. (2011) for extra-tropical forests
EF_{CO_2}	1580 ± 160	1640 ± 160	1650 ± 170	1640 ± 160	1590 ± 160	1620 (±30)	1637 ± 71	1509 ± 98
EF_{CO}	136 ± 22	106 ± 17	102 ± 16	112 ± 18	133 ± 21	118 (±16)	89 ± 32	122 ± 44
EF_{CH_4}	4.8 ± 0.9	2.9 ± 0.5	2.7 ± 0.4	2.7 ± 0.5	4.5 ± 0.8	3.5 (±1.1)	3.9 ± 2.4	5.7 ± 3.2
$EF_{\text{C}_2\text{H}_4}$	1.6 ± 0.3	1.1 ± 0.2	1.1 ± 0.2	1.1 ± 0.2	1.5 ± 0.3	1.3 (±0.3)	1.1 ± 0.4	1.4 ± 0.4
$EF_{\text{H}_2\text{CO}}$	2.4 ± 0.4	1.5 ± 0.3	1.4 ± 0.2	1.7 ± 0.3	1.8 ± 0.3	1.7 (±0.4)	2.3 ± 1.1	1.9 ± 1.1
$EF_{\text{CH}_3\text{OH}}$	4.0 ± 0.8	1.6 ± 0.3	1.5 ± 0.3	1.6 ± 0.3	3.2 ± 0.6	2.4 (±1.2)	1.9 ± 1.4	2.7 ± 1.8
$EF_{\text{CH}_3\text{COOH}}$	5.5 ± 1.2	2.8 ± 0.6	2.6 ± 0.6	3.6 ± 0.8	4.8 ± 1.0	3.8 (±1.3)	2.0 ± 1.6	4.1 ± 3.0
EF_{HCOOH}	0.7 ± 0.2	0.26 ± 0.06	0.29 ± 0.07	0.36 ± 0.09	0.43 ± 0.11	0.4 (±0.2)	0.35 ± 0.33	0.54 ± 0.47
EF_{NH_3}	2.2 ± 0.5	1.0 ± 0.2	1.4 ± 0.3	0.8 ± 0.2	3.1 ± 1.1	1.7 (±0.9)	0.78 ± 0.82	2.5 ± 2.4
$EF_{\text{N}_2\text{O}}$				0.21 ± 0.04	0.09 ± 0.01	0.15 (±0.09)	0.16 ± 0.21	0.38 ± 0.35
$EF_{\text{C}_2\text{H}_6}$					0.5 ± 0.2	0.5	1.1 ± 0.7	1.7 ± 1.0

Title Page

Abstract Introduction

Conclusions References

Tables Figures

⏪ ⏩

◀ ▶

Back Close

Full Screen / Esc

Printer-friendly Version

Interactive Discussion



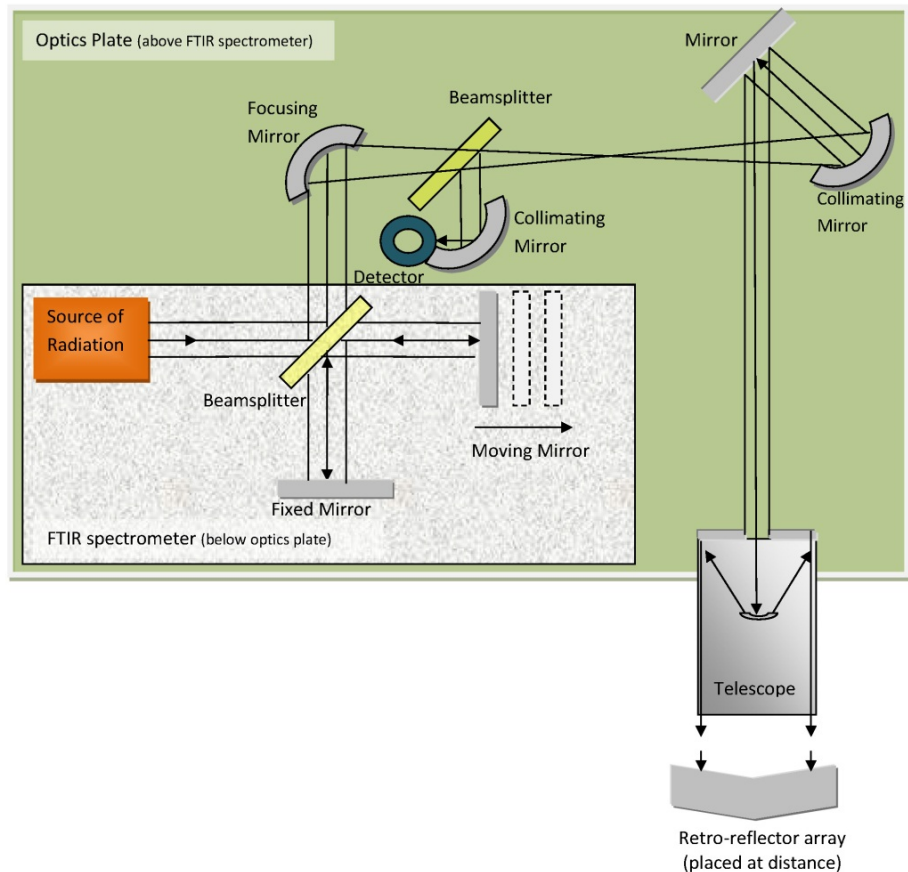


Fig. 1. Schematic of the instrumental set-up, showing a basic Fourier transform spectrometer and the optics that have been mounted on the top plate to steer the modulated radiation from the spectrometer through the telescope to the distant retro-reflector array and back again to be focused onto the detector.

New emission factors for Australian vegetation fires

C. Paton-Walsh et al.

Title Page

Abstract

Introduction

Conclusions

References

Tables

Figures

◀

▶

◀

▶

Back

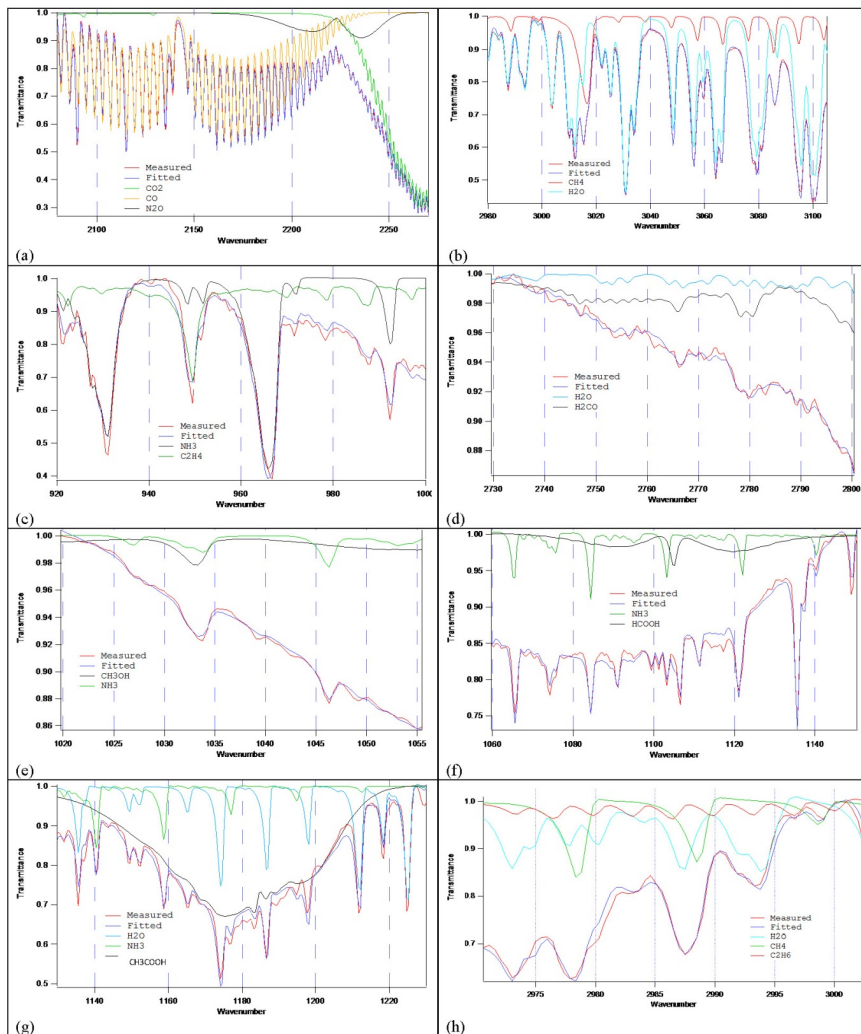
Close

Full Screen / Esc

Printer-friendly Version

Interactive Discussion





New emission factors for Australian vegetation fires

C. Paton-Walsh et al.

Title Page

Abstract

Introduction

Conclusions

References

Tables

Figures

◀

▶

◀

▶

Back

Close

Full Screen / Esc

Printer-friendly Version

Interactive Discussion



Fig. 2. Plots of MALT fits of simulated to measured spectra, showing the main gases contributing to the absorption features in each spectral region. **(a)** Example fit in 2080–2270 cm^{-1} region fitting CO_2 , CO , N_2O , **(b)** Example fit in 2980–3105 cm^{-1} region fitting CH_4 **(c)** Example fit in 920–1000 cm^{-1} region fitting C_2H_4 , NH_3 , **(d)** Example fit in 2730–2800 cm^{-1} region fitting H_2CO , **(e)** Example fit in 1020–1055 cm^{-1} region fitting CH_3OH , **(f)** Example fit in 1060–1150 cm^{-1} region fitting HCOOH , **(g)** Example fit in 1130–1230 cm^{-1} region fitting CH_3COOH , **(h)** Example fit in 2971–3002 cm^{-1} region fitting C_2H_6 .

New emission factors for Australian vegetation fires

C. Paton-Walsh et al.

[Title Page](#)[Abstract](#)[Introduction](#)[Conclusions](#)[References](#)[Tables](#)[Figures](#)[◀](#)[▶](#)[◀](#)[▶](#)[Back](#)[Close](#)[Full Screen / Esc](#)[Printer-friendly Version](#)[Interactive Discussion](#)



Fig. 3. The instrumental set-up for open-path FTIR measurements of smoke at the different burns is shown: **(a)** Max Allen Drive – looking up towards retro-reflectors; **(b)** Gibberagong – line of sight along fire break; **(c)** Aberoo Creek (Day 1) – line of sight by main road to Sydney; **(d)** Aberoo Creek (Day 2) – spectrometer and telescope on fire trail; **(e)** Gulguer Nature Reserve – line of sight through burning understory and **(f)** Alford's Point – small arrow shows line of sight at top of escarpment, large arrow shows wind direction.

**New emission factors
for Australian
vegetation fires**

C. Paton-Walsh et al.

Title Page	
Abstract	Introduction
Conclusions	References
Tables	Figures
⏪	⏩
◀	▶
Back	Close
Full Screen / Esc	
Printer-friendly Version	
Interactive Discussion	



New emission factors
for Australian
vegetation fires

C. Paton-Walsh et al.

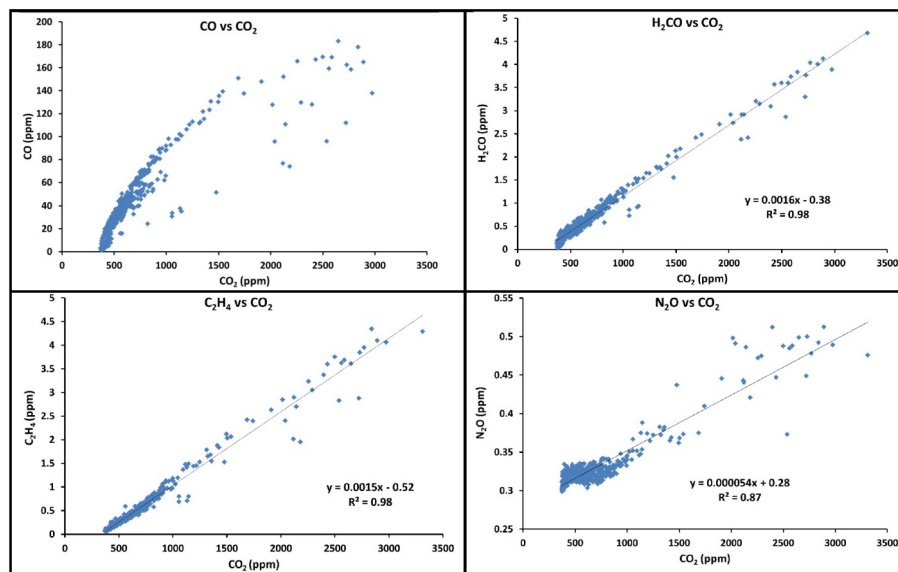


Fig. 4. Example correlation plots with respect to CO₂ from the Alford's Point burn. Upper left hand panel is CO vs. CO₂; upper right hand panel is H₂CO vs. CO₂; lower left hand panel is C₂H₄ vs. CO₂ and lower right hand panel is N₂O vs. CO₂.

[Title Page](#)[Abstract](#)[Introduction](#)[Conclusions](#)[References](#)[Tables](#)[Figures](#)[◀](#)[▶](#)[◀](#)[▶](#)[Back](#)[Close](#)[Full Screen / Esc](#)[Printer-friendly Version](#)[Interactive Discussion](#)

New emission factors
for Australian
vegetation fires

C. Paton-Walsh et al.

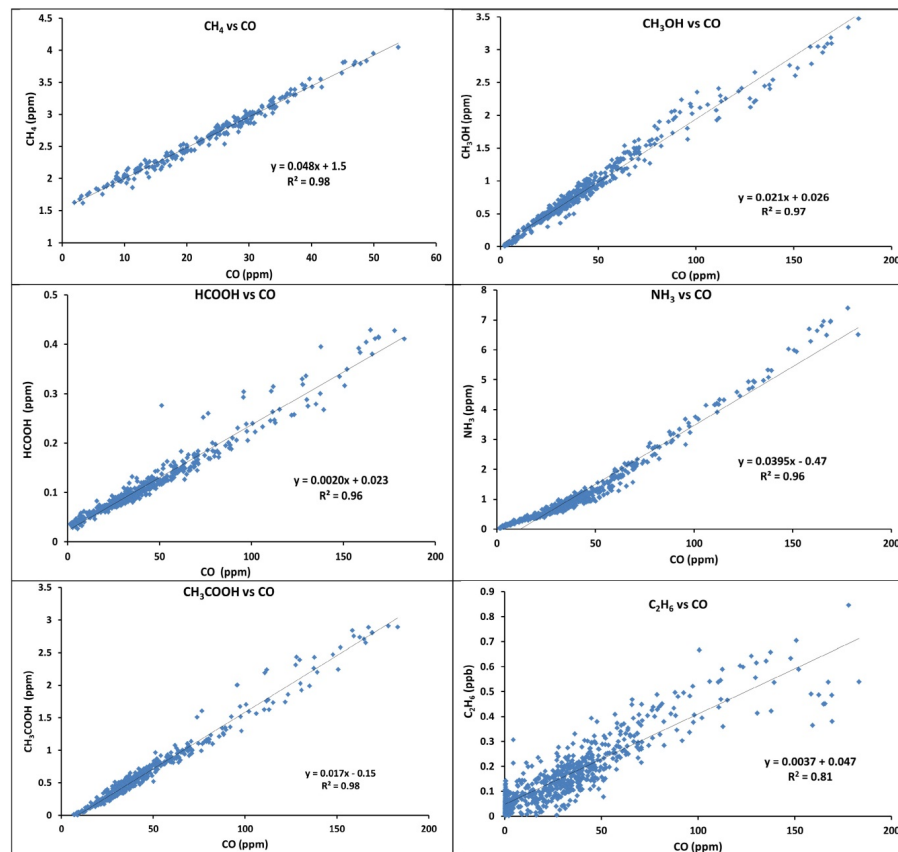


Fig. 5. Example correlation plots with respect to CO. Upper left hand panel is CH_4 vs. CO from Turramurra burn; All other data is from Alford's Point: upper right hand panel is CH_3OH vs. CO; middle left hand panel is HCOOH vs. CO; middle right hand panel is NH_3 vs. CO; lower left hand panel is CH_3COOH vs. CO and lower right hand panel is C_2H_6 vs. CO..

[Title Page](#)[Abstract](#)[Introduction](#)[Conclusions](#)[References](#)[Tables](#)[Figures](#)[◀](#)[▶](#)[◀](#)[▶](#)[Back](#)[Close](#)[Full Screen / Esc](#)[Printer-friendly Version](#)[Interactive Discussion](#)

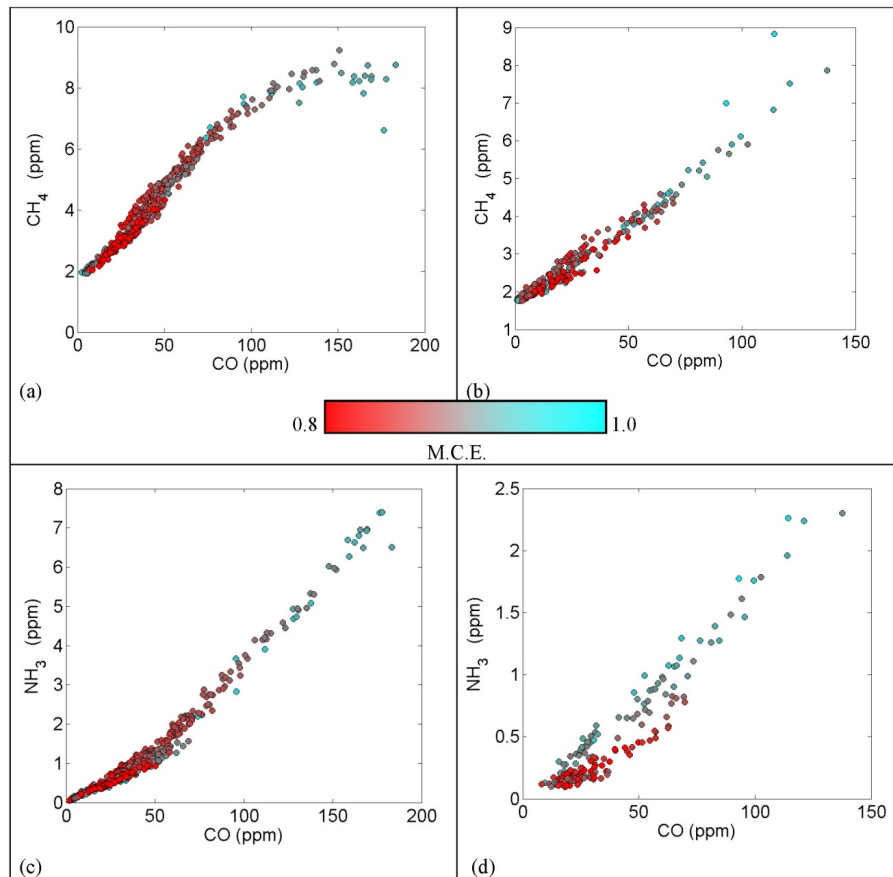


Fig. 6. Correlation plots illustrating anomalous behaviour in CH₄ vs. CO at Alford's Point and NH₃ vs. CO at both sites: **(a)** CH₄ vs. CO from Alford's Point; **(b)** CH₄ vs. CO from Gulguer Nature Reserve; **(c)** is NH₃ vs. CO from Alford's Point; **(d)** NH₃ vs. CO from Gulguer Nature Reserve. Points are coloured by MCE from red = 0.8 to blue = 1.0.